

High-Resolution Global Analysis of the Influences of Bas1 and Ino4 Transcription Factors on Meiotic DNA Break Distributions in *Saccharomyces cerevisiae*

Xuan Zhu^{*,†} and Scott Keeney^{*,†,‡,1}

^{*}Molecular Biology Program and [‡]Howard Hughes Medical Institute, Memorial Sloan Kettering Cancer Center, New York, New York 10065, and [†]Weill Cornell Graduate School of Medical Sciences, New York, New York 10065

ORCID ID: 0000-0002-1283-6417 (S.K.)

ABSTRACT Meiotic recombination initiates with DNA double-strand breaks (DSBs) made by *Spo11*. In *Saccharomyces cerevisiae*, many DSBs occur in “hotspots” coinciding with nucleosome-depleted gene promoters. Transcription factors (TFs) stimulate DSB formation in some hotspots, but TF roles are complex and variable between locations. Until now, available data for TF effects on global DSB patterns were of low spatial resolution and confined to a single TF. Here, we examine at high resolution the contributions of two TFs to genome-wide DSB distributions: *Bas1*, which was known to regulate DSB activity at some loci, and *Ino4*, for which some binding sites were known to be within strong DSB hotspots. We examined fine-scale DSB distributions in TF mutant strains by deep sequencing oligonucleotides that remain covalently bound to *Spo11* as a byproduct of DSB formation, mapped *Bas1* and *Ino4* binding sites in meiotic cells, evaluated chromatin structure around DSB hotspots, and measured changes in global messenger RNA levels. Our findings show that binding of these TFs has essentially no predictive power for DSB hotspot activity and definitively support the hypothesis that TF control of DSB numbers is context dependent and frequently indirect. TFs often affected the fine-scale distributions of DSBs within hotspots, and when seen, these effects paralleled effects on local chromatin structure. In contrast, changes in DSB frequencies in hotspots did not correlate with quantitative measures of chromatin accessibility, histone H3 lysine 4 trimethylation, or transcript levels. We also ruled out hotspot competition as a major source of indirect TF effects on DSB distributions. Thus, counter to prevailing models, roles of these TFs on DSB hotspot strength cannot be simply explained via chromatin “openness,” histone modification, or compensatory interactions between adjacent hotspots.

KEYWORDS *Spo11*; meiotic recombination; double-strand break; transcription factor; chromatin

MEIOSIS is a specialized cell division in which one round of DNA replication is followed by two successive rounds of chromosome segregation to produce haploid gametes from diploid cells. In meiotic prophase, most sexually reproducing organisms use homologous recombination to form physical connections between homologous chromosomes that are essential for accurate chromosome segregation (Petronczki *et al.* 2003). Recombination also disrupts linkage of sequence polymorphisms on the same chromosome and thus promotes genome diversity and evolution (Kauppi *et al.* 2004).

Recombination is initiated by the programmed formation of DNA double-strand breaks (DSBs). Approximately 150–200 DSBs are formed per meiosis in *Saccharomyces cerevisiae* (Buhler *et al.* 2007; Chen *et al.* 2008; Mancera *et al.* 2008; Pan *et al.* 2011), generated by a dimer of the topoisomerase-like protein *Spo11* (Bergerat *et al.* 1997; Keeney *et al.* 1997). After break formation, *Spo11* remains covalently bound to the 5′ DNA strand termini (de Massy *et al.* 1995; Keeney and Kleckner 1995; Liu *et al.* 1995). Single-stranded nicks nearby then release *Spo11* still bound to a short oligonucleotide (*Spo11*-oligo complexes; Figure 1A) (Neale *et al.* 2005) and permit further 5′-to-3′ resection to generate 3′ single-stranded tails, which are substrates for strand exchange proteins (Sun *et al.* 1991; Schwacha and Kleckner 1994; Goldfarb and Lichten 2010; Zakharyevich *et al.* 2010).

Copyright © 2015 by the Genetics Society of America

doi: 10.1534/genetics.115.178293

Manuscript received May 17, 2015; accepted for publication August 2, 2015; published Early Online August 4, 2015.

Supporting information is available online at www.genetics.org/lookup/suppl/doi:10.1534/genetics.115.178293/-/DC1.

¹Corresponding author: Memorial Sloan Kettering Cancer Center, 1275 York Ave., Box 97, New York, NY 10065. E-mail: s-keeney@ski.mskcc.org

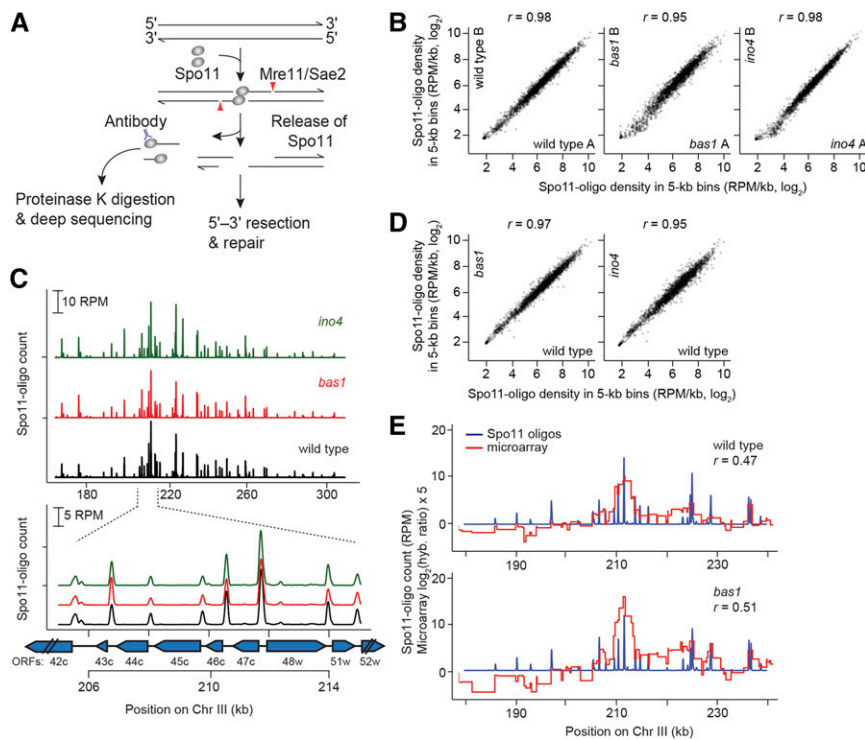


Figure 1 Spo11-oligo mapping in *bas1* and *ino4* mutants. (A) Formation and processing of meiotic DSBs (Spo11-oligo mapping method on left). (B) Quantitative reproducibility of Spo11-oligo maps. Comparisons are shown for individual wild-type, *bas1*, or *ino4* datasets. Spo11 oligos were summed in nonoverlapping 5-kb bins and expressed as RPM per kilobase (plotted on a log scale). Correlation coefficients (Pearson's r) are shown on the top. (C) Top, *bas1* and *ino4* mutations do not cause widespread change in the large-scale patterns of the DSB landscape. Bottom, DSBs form at the same hotspots in *bas1* and *ino4* as in wild type. Spo11-oligo counts here and in E are the per-base pair frequency, smoothed with a 201-bp Hann window. Positions of open reading frames are indicated by blue arrows. (D) Comparison between wild-type and TF mutant datasets. For each genotype, Spo11-oligo maps were averaged from biological replicates. (E) The Spo11-oligo map agrees with previous *rad50S* Spo11 ChIP microarray analysis (Mieczkowski *et al.* 2006) but provides higher resolution. A representative genomic region is shown. The value for each microarray probe is plotted along the length of sequence covered by the probe. The correlation coefficient was calculated between the normalized microarray signal and the sum of Spo11-oligo counts within 2 kb on either side of each microarray probe.

The distribution of meiotic DSBs across the *S. cerevisiae* genome is highly nonrandom (Baudat and Nicolas 1997; Gerton *et al.* 2000; Borde *et al.* 2004; Blitzblau *et al.* 2007; Buhler *et al.* 2007; Pan *et al.* 2011). There are large DSB-hot and -cold domains (tens of kilobases), within which are short regions called hotspots (typically several hundred base pairs wide), where DSBs preferentially form. Most hotspots in *S. cerevisiae* coincide with the nucleosome-depleted regions at gene promoters (Wu and Lichten 1994; Baudat and Nicolas 1997; Pan *et al.* 2011). The global DSB landscape is shaped by a hierarchical combination of factors, including whole chromosome variation, large subchromosomal domains, presence of cohesins and other chromosome structure proteins, local chromatin structure, and histone modification (Lichten and Goldman 1995; Petes 2001; Kauppi *et al.* 2004; Lichten and de Massy 2011; Pan *et al.* 2011; Acquaviva *et al.* 2013; de Massy 2013; Sommermeyer *et al.* 2013).

In some cases, DSB hotspot activity has been shown to depend on the binding of sequence-specific transcription factors (TFs), *e.g.*, at the *HIS4* locus in *S. cerevisiae* and the *ade6-M26* allele in *Schizosaccharomyces pombe* (Schuchert *et al.* 1991; White *et al.* 1991; Kon *et al.* 1997; Steiner *et al.* 2002). However, the role of TFs in shaping genome-wide DSB patterns is complex and poorly defined. In certain *S. cerevisiae* strains, the *HIS4* promoter displays strong hotspot activity that requires the binding of TFs *Bas1*, *Bas2*, and *Rap1* (White *et al.* 1991). A *bas1* null mutation reduces DSB activity at a number of chromosomal sites, but it also causes increased DSB frequency at many other sites (Mieczkowski *et al.* 2006). Thus, the effect of *Bas1* on DSB formation is context dependent,

and local DSB stimulation by this TF at *HIS4* cannot be simply extrapolated as a general feature to all genomic loci. Moreover, loci whose DSB activity changes in *bas1* mutants are poorly correlated with *Bas1* binding sites defined by chromatin immunoprecipitation (ChIP), suggesting *Bas1* has both direct and indirect roles in DSB regulation (Mieczkowski *et al.* 2006).

Even in those instances where DSB hotspot activity is clearly linked to TF binding, the nature of this link has remained elusive. Like most yeast promoters, the *HIS4* promoter exhibits hypersensitivity to DNase I digestion of chromatin, but it becomes nuclease resistant when it loses DSB hotspot activity in *bas1 bas2* double mutants (Fan and Petes 1996). Another example is the *PHO5* promoter, which is bound by the TF *Pho4* (Wu and Lichten 1994). When *PHO5* transcription is inhibited by deleting *Pho4*, its promoter is occupied by a well-positioned nucleosome array and meiotic DSBs are detected as a narrow band by Southern blot. However, in the transcriptionally induced state, the nucleosomes are absent and the DSB band becomes dramatically wider across the whole nucleosome-depleted promoter. Thus, TF binding can promote DSB formation nearby, possibly via establishing an open chromatin structure in the surrounding area. However, the available data are anecdotal: *HIS4* and *PHO5* are the only TF-dependent hotspots for which the effect of TFs on meiotic DNA accessibility and DSBs has been examined in budding yeast. It is unknown whether TF binding can cause DNA accessibility change at DSB sites in all TF-affected hotspots.

Thus far, *Bas1* is the only TF that has been studied genome-wide for its influence on meiotic DSB distribution. *Bas1* is a Myb-related TF involved in the expression of genes acting

in the adenine and histidine biosynthetic pathways (Arndt *et al.* 1987; Daignan-Fornier and Fink 1992; Denis *et al.* 1998). *Bas1* binds to a site containing a GAGTCA motif found in the *ADE2* and *ADE5,7* promoters (Hovring *et al.* 1994). This motif is required for regulation of *ADE2* by *Bas1* and another TF *Bas2/Pho2* (Daignan-Fornier and Fink 1992). It has been proposed that formation of a complex between *Bas1* and *Bas2* unmasks an activator function of *Bas1*, but there may be other partners that can bind *Bas1* as well (Denis and Daignan-Fornier 1998). *Bas1* and *Bas2* also regulate several genes involved in one-carbon metabolism, such as *GLN1*, *SHM2*, and *MTD1* (Denis and Daignan-Fornier 1998; Gelling *et al.* 2004).

Meiotic DSBs were previously mapped genome-wide in a *bas1* mutant by microarray hybridization of *Spo11*-attached DNA from a *rad50S* mutant (Mieczkowski *et al.* 2006). In the *rad50S* background, *Spo11* is not released from DSB ends and thus repair is blocked and DSBs accumulate (Alani *et al.* 1990; Keeney *et al.* 1997). A total of 153 open reading frames (ORFs) were identified as regions with different DSB frequency between wild type and *bas1*, but the spatial resolution (usually several kilobases) was not high enough to precisely locate DSB hotspots in these regions (Mieczkowski *et al.* 2006). Besides *bas1*, there are no genome-wide DSB maps of other TF mutants.

In this study, we wished to more precisely define the contributions of specific TFs to global DSB patterns. We examined a *bas1* mutant because, while it is known to affect DSBs, nucleotide-resolution information about changes in DSB patterns was lacking. To determine whether another TF affects break formation similarly to *Bas1*, we also examined an *ino4* mutant. *Ino4* motifs were previously found to be enriched in strong DSB hotspots (Pan *et al.* 2011), but it was unknown if *Ino4* stimulates DSB activity in those hotspots. *Ino4* controls genes involved in phospholipid synthesis and is required for derepression of inositol/choline-regulated genes such as *INO1*, *CHO1*, *CHO2*, and *OPI3* (Santiago and Mamoun 2003). *Ino4* forms a complex with *Ino2* and binds the inositol-choline-responsive element through a basic helix-loop-helix domain (Schwank *et al.* 1995).

Here, we ask the following questions: Is the context dependence for DSB frequency modulation seen for *Bas1* a unique situation, or does it also hold for another TF? Are TF effects on DSB frequency mediated principally via opening or closing of local chromatin structure, as has been hypothesized (Wu and Lichten 1994; Mieczkowski *et al.* 2006; Lichten 2008)? Are indirect effects of TFs mediated by local competition between hotspots? And, separate from effects on DSB numbers, do TFs influence fine-scale DSB patterns around their binding sites, and if so, how?

Materials and Methods

Yeast strains and culture methods

Strains used in this study are of the SK1 background and are listed in Supporting Information, Table S1. The *bas1* and *ino4*

deletions were made by replacing the coding sequence with the hygromycin B phosphotransferase gene (*hphMX4*). The *sae2* deletion was made by replacing the coding sequence with the ClonNAT resistance gene (*natMX*). Gene disruption was verified by PCR and Southern blotting. The *SPO11-FLAG* construct was provided by Kunihiko Ohta (Kugou *et al.* 2009). All mutants analyzed were moved into the desired tester strain backgrounds by crossing and tetrad dissection. Synchronous meiotic cultures were prepared as described (Alani *et al.* 1990; Padmore *et al.* 1991). Briefly, cells were grown in YPA (1% yeast extract, 2% Bacto Peptone, 1% potassium acetate) for 13.5–14 hr at 30° (starting OD₆₀₀ = 0.2, ending OD₆₀₀ = 2~4), harvested, resuspended in 2% potassium acetate (OD₆₀₀ = 4.5~6), and sporulated at 30°. Null *bas1* and *ino4* mutants show normal division kinetics and spore viability (data not shown).

Spo11-oligo mapping

Spo11-oligo mapping was performed with 3000–4000 OD₆₀₀ units of cells harvested at 4 hr in meiosis from cultures prepared as described above, except with supplementation of YPA with 0.001% antifoam 204. Cell lysates were prepared by grinding frozen cell paste in a bead mill, similar to methods described (Thacker *et al.* 2014). The lysate was then diluted with an equal volume of 2× immunoprecipitation (IP) buffer (2% Triton X-100, 30 mM Tris-HCl, pH 8.0, 300 mM NaCl, 2 mM EDTA) and incubated with protein G agarose beads (Roche) for mock IP (4 hr at 4° mixing end over end, 400 μl beads per 50 ml extract). Supernatant was removed into fresh tubes and the mock IP beads were stored on ice. The supernatant was incubated with 80 μl anti-FLAG antibody (Sigma) and 400 μl protein G agarose beads per 50 ml of extract for 4 hr at 4° mixing end over end, and then beads were recovered. Mock and IP beads were washed three times with cold 1× IP buffer. Protein was eluted from mock or IP beads with 400 μl 2× NuPAGE LDS buffer (Invitrogen) by boiling for 5 min, followed by a second elution with 400 μl 0.5× NuPAGE LDS buffer. The eluates were combined and diluted with 800 μl of 2× IP buffer, then incubated with 125 μl fresh protein G agarose beads (mock) or 25 μl anti-FLAG antibody plus 125 μl protein G agarose beads (IP), 4° overnight with end-over-end rotation.

The beads were recovered and resuspended in 400 μl proteinase K buffer (100 mM Tris-HCl, pH 7.4, 1 mM EDTA, 0.5% SDS, 1 mM CaCl₂) and 100 μg purified proteinase K, and incubated overnight at 50° with end-over-end rotation. The supernatant was collected using a SPIN-X tube (Corning) and ethanol precipitated with 0.3 volume of 9 M ammonium acetate, 10 μg of DNA-free glycogen, and 2.5 volumes of 100% ethanol. *Spo11* oligos were then quantified and used for library preparation as described (Thacker *et al.* 2014). Sequencing was performed using Illumina HiSeq in the Memorial Sloan Kettering Cancer Center (MSKCC) Integrated Genomics Operation core facility.

Statistical analyses were performed using R version 3.0.1 (<http://www.r-project.org/>). Clipping of library adapters

and mapping of reads to the *sacCer2* genome assembly was performed using a custom pipeline as described (Pan *et al.* 2011; Thacker *et al.* 2014). Sequence read totals and mapping statistics are described in Table S2. After mapping, the reads were separated into unique and multiple mapping sets, but only uniquely mapping reads were analyzed in this study (multiple mapping reads constituted a small minority of the total) (Table S2). Each map was normalized to the total number of uniquely mapped reads (reads per million, RPM; excluding reads mapping to mitochondrial DNA or the 2 μ plasmid), then maps for biological replicates were averaged. Hotspot calling was performed as described (Pan *et al.* 2011) on a merged map made by combining the averages of the wild-type, *bas1*, and *ino4* maps. Hotspot positions and their *Spo11*-oligo counts are compiled in Table S3. In analyses evaluating the fold change in TF mutants, we assumed genome-wide numbers of DSBs are approximately the same in wild type and in the TF mutants, which agreed with direct DSB measurement by Southern blotting (Figure 2, G, H, and K–N). The *bas1* B, *bas1* C, *bas1* D, *ino4* A, and *ino4* B datasets contained a small number of spurious reads (<0.3% of total in *bas1* dataset B, <0.04% of total in the other datasets) at positions 244,583 bp and 244,584 bp on chromosome V as well as 152,223 bp on chromosome III, likely from contamination of the *Spo11*-oligo sequencing libraries with PCR primers from those loci. These reads were deleted from the maps. Sequence reads and compiled *Spo11*-oligo maps have been submitted to the Gene Expression Omnibus (GEO) repository.

Detection of meiotic DSBs by Southern blot

Genomic DNA was prepared in agarose plugs as described (Borde *et al.* 2000; Murakami *et al.* 2009). DSB analyses at individual hotspots were performed as described (Murakami *et al.* 2009; Pan *et al.* 2011). Restriction enzymes and primer sequences for amplification of probes were as follows: *GCV2*–*MRPS17* hotspot, *StuI*, *MRPS17* probe (5'-TCCATCATGACGTGCTTTCT, 5'-AGCCCAAAGGCAAAGAAT); *GAT2*–*GID8* hotspot, *XbaI*, *PSO2* probe (5'-GCTTTCGTCACATGTCAT, 5'-TCGAAGCAACGCCAAAATGA); *SHM2* hotspot, *NcoI*-HF, *SHM2* probe (5'-GAGAATCGGTACCGTTGGAA, 5'-CAGGTGTCATCCCATCTCCT); *CHO2* hotspot, *XbaI*, *CYS4* probe (5'-CTGGTGGGACTATTAGCGGT, 5'-AAGAGTCAAAACGGGCC AAC); *ADO1*–*SOD1* hotspot, *XbaI*, *YPS25* probe (5'-AATAGAGCAAGCTTTCGGGC, 5'-ACCCGTCAACCAATTCTTT); and *FAS1* hotspot, *XbaI*, *ASH1* probe (5'-CGCTTAGAGGAGTAGAGGCC, 5'-GCTTGGAGTGTATGCCTTGG). Blots were quantified by phosphorimager.

ChIP-seq to define *Bas1* and *Ino4* binding sites

Bas1 and *Ino4* were C-terminally tagged with eight copies of the Myc epitope (*BAS1*-Myc and *INO4*-Myc). ChIP was performed as described (Murakami and Keeney 2014). ChIP efficiencies (percent of input) were measured by qPCR. DNA from ChIP and input samples collected from the tagged strains were sequenced (50-bp paired-end reads) on the

HiSeq platform (Illumina). Reads were mapped to the *S. cerevisiae* *sacCer2* genome assembly using BWA mem (version 0.7.5a-r405) to generate coverage maps for each dataset. To remove regions with spurious mapping, the maps from the input samples of the *BAS1*-myc or *INO4*-Myc strains were used to define ad hoc “mask regions” where the coverage was out of a fixed range (>5 SD from mean coverage for *Bas1* maps, and >4 SD from mean coverage for *Ino4* maps; these values were chosen to achieve similar extents of mask coverage for the two sets of samples, accommodating fluctuation of input signals between samples, presumably due to experimental variation in crosslinking efficiency, sonication, and chromatin solubilization). Masks covered 7.2% and 6.6% of the genome for *Bas1* and *Ino4* maps, respectively; 74.2% of the *Bas1* mask regions overlapped *Ino4* mask regions (*i.e.*, 81.6% of the *Ino4* mask regions were accounted for). These regions were censored from further analysis. Coverage was normalized to the mean coverage calculated from the masked map and made into ChIP/input ratio. The ratio maps were smoothed using a 501-bp Parzen (triangular) sliding window. Using the smoothed maps, peaks were called using a threshold 2.0 \times genome average. *De novo* motif discovery on sequences corresponding to windowed peaks was performed using MEME (Machanick and Bailey 2011). Matches to position weight matrices for each motif were called using MEME default settings.

Micrococcal nuclease digestion of chromatin

Isolation of nuclei, micrococcal nuclease (MNase) digestion of chromatin, and proteinase K treatment were performed as described (Keeney and Kleckner 1996; Sasaki *et al.* 2013). After proteinase K treatment, reactions were precipitated with an equal volume of isopropanol and dissolved in 50 μ l TE buffer. *SHM2* and *GCV2* hotspots were analyzed using the same restriction enzymes and probes as in direct DSB measurement above. Additional restriction enzymes and primer sequences for amplification of probes were as follows: *GAT2*–*GID8* hotspot, *XhoI*, *GAT2* probe (5'-CGCGCCTCTTCAAAA GTTAC, 5'-TGGTCCCTTTCTCCATTCTG); *CHO2* hotspot, *BmgBI* (isoschizomer of *BtrI*), *CHO2* probe (5'-TTGATGA AAGCAAGAACTCCA, 5'-CTCCAATGACCACCTGATCC); *ADO1*–*SOD1* hotspot, *HpaI*, *URA8* probe (5'-ACCACGTTCC CTTATTGCTG, 5'-TCCACCAGGAACCAAAATTC); and *FAS1* hotspot, *SalI*-HF, *FAS1* probe (5'-TGGTGCGAAGAATCTAGT CG, 5'-CTCGGAAATGGAACCTGAAA).

ChIP-seq of histone H3 lysine 4 trimethylation

Approximately 250 OD units of cells were collected for each sample. Cells were crosslinked with 1% formaldehyde for 15 min and quenched with 125 mM glycine for 5 min at room temperature. Cells were collected and disrupted by bead beating in 200 μ l lysis buffer (50 mM HEPES-NaOH, pH 7.5, 150 mM NaCl, 2 mM EDTA, 1% Triton X-100, 0.1% Na-deoxycholate). Chromatin was prepared and washed with MNase reaction buffer (10 mM Tris-HCl, pH 7.5, 50 mM NaCl, 5 mM MgCl₂, 1 mM CaCl₂, 1 mM β -mercaptoethanol,

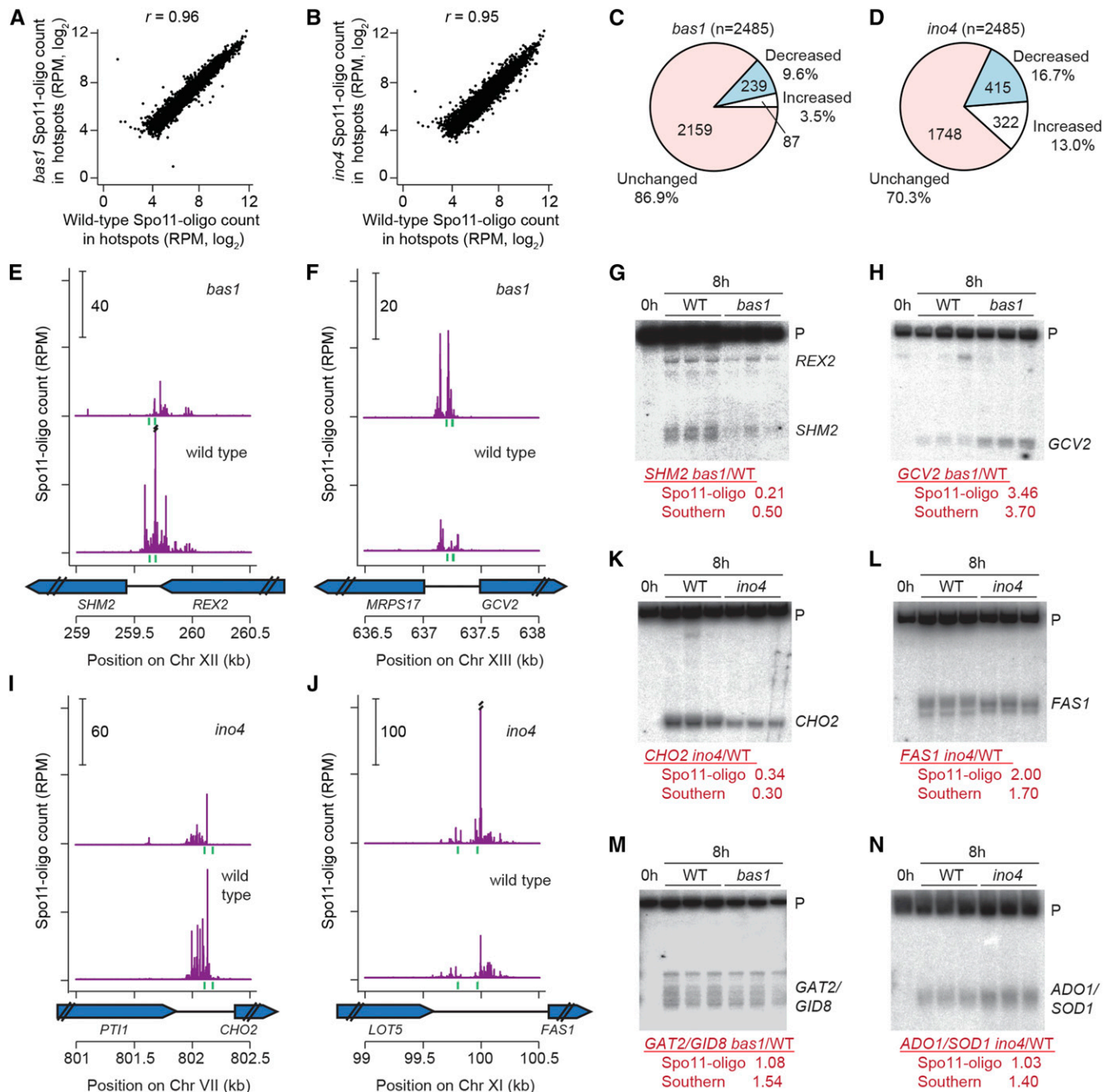


Figure 2 Effects of *bas1* and *ino4* mutations on DSB activity at individual hotspots. (A and B) Comparisons between wild type and TF mutants for all hotspots. (C and D) Proportion of hotspots that displayed at least a 20% change in Spo11-oligo counts relative to wild type. (E, F, I, and J) Spo11 oligos in hotspots at the promoters of *SHM2* (E), *GCV2* (F), *CHO2* (I), and *FAS1* (J). Double slashes indicate where Spo11-oligo counts are off scale. Green vertical ticks indicate sequence matches to Bas1 (E and F) or Ino4 (I and J) binding motifs. (G, H, and K–N) Southern blot results confirming the Spo11-oligo data for hotspots at the promoters of *SHM2* (G), *GCV2* (H), *CHO2* (K), *FAS1* (L), *GAT2–GID8* (M), and *ADO1–SOD1* (N). Genomic DNA was purified from three independent 8-hr *sae2Δ* cultures for each genotype and analyzed by Southern blotting and indirect end labeling. Fold change (mutant/wild type) for each hotspot is shown below the blots. P, parental.

0.1% Igepal CA-630 (Sigma-Aldrich) and digested to predominantly mono-nucleosomes with 2 units MNase at 37° for 30 min. ChIP-seq was then performed on nucleosomes with anti-H3 (Abcam, ab1791) or anti-H3 lysine 4 trimethylation (H3K4me3) (Abcam, ab8580) as described (Zhang *et al.* 2011b; Murakami and Keeney 2014). Reads were

mapped to the *sacCer2* genome assembly using BWA mem (version 0.7.5a-r405). The midpoint position of each paired-end read was extracted. The coordinate of the midpoints was shifted 73 bp toward both the 5' and 3' ends to generate nucleosome coverage maps. Each H3 or H3K4me3 map was normalized to the mean coverage. H3K4me3 enrichment was

measured by taking the ratio of H3K4me3 ChIP signal to H3 ChIP signal.

RNA-seq

Deep sequencing of RNA (RNA-seq) was performed on two biological replicates each for wild type, *bas1*, and *ino4*. For each sample, 15 OD₆₀₀ units of cells were collected at 4 hr in meiosis. Cells were resuspended in 500 μ l Complete Buffer A (50 mM sodium acetate pH 5.2, 10 mM EDTA, 1% SDS) and 750 μ l of phenol equilibrated with Complete Buffer A was added. Cells were disrupted by incubating at 65° for 5 min with vortexing for 10 s every 1.5 min, and then placed on ice for 3 min. After spinning in a mini centrifuge at 13,000 rpm for 6 min, the bottom layer was removed and fresh phenol was added to the top layer. Incubation and vortexing were repeated, except that the top layer was then transferred to a new 1.5-ml tube. RNA was purified by two rounds of phenol/chloroform extraction, one round of chloroform extraction, and ethanol precipitation. Precipitates were dissolved in 100 μ l TE (10 mM Tris-HCl pH 6.8, 1 mM EDTA). Messenger RNA (mRNA) was enriched by poly-A selection and sequenced using Illumina HiSeq in the Genomics Resources Core Facility of Weill Cornell Medical College. Reads were mapped to the *S. cerevisiae* sacCer2 genome assembly using the Spliced Transcripts Alignment to a Reference (STAR) software (Dobin *et al.* 2013). Transcriptome assembly and differential expression analysis were performed using the Cufflinks software (Trapnell *et al.* 2010) and R Cummebund package (<http://compbio.mit.edu/cummeRbund/>).

Data availability

Strains are available upon request. Next-generation sequencing data were deposited at the Gene Expression Omnibus (GEO) under accession nos. GSE67910 (*Spo11*-oligo mapping), GSE67912 (*Bas1* and *Ino4* ChIP-seq), GSE67907 (H3K4me3 ChIP), and GSE70911 (RNA-seq).

Results

High-resolution maps of meiotic DSBs in *bas1* and *ino4* mutants

Each covalently bound *Spo11* oligo is a unique tag from a DSB site, so sequencing *Spo11* oligos generates quantitative, high-resolution DSB maps (Pan *et al.* 2011). *Spo11*-oligo maps from biological replicate cultures of wild type and *bas1* and *ino4* mutants agreed well with each other (Pearson's $r = 0.92$ – 0.98 ; Figure 1B) and thus were averaged (after normalization to millions of reads mapped, RPM) into consensus maps for further analysis.

The DSB landscape is shaped by a combination of many factors that operate at different scales. At large scales (tens of kilobases), *bas1* and *ino4* *Spo11*-oligo maps agreed with the wild-type map (Figure 1C, top). At small scales (<1 kb), DSB hotspots are usually located in nucleosome-depleted promoters. This pattern was retained in *bas1* and *ino4* mutants,

in that DSBs formed in the same hotspots (Figure 1C, bottom). The correlation of *Spo11*-oligo density in 5-kb bins was high across the genome (Pearson's $r = 0.95$ – 0.97) (Figure 1D). Thus, these TF mutants do not grossly alter the global DSB landscape.

To compile a list of hotspots to facilitate direct comparison of each mutant to wild type, we pooled the averaged wild-type map, the averaged *bas1* map, and the averaged *ino4* map, then called hotspots (clusters of *Spo11* oligos) on this combined map using a previously described algorithm (Pan *et al.* 2011). We identified 3994 hotspots (Table S3). Of these, 3524 (88.2%) overlapped the 3600 hotspots previously identified in wild type (Pan *et al.* 2011) (*i.e.*, 97.9% of the previous hotspots were accounted for). The extra hotspots in the current study were weak hotspots (≤ 250 RPM, equivalent to a DSB frequency of $\leq 0.45\%$ of DNA, as estimated by comparing Southern blot data to *Spo11*-oligo counts) (Pan *et al.* 2011), probably emerging from the greatly increased sequencing depth in the current study.

The wild-type and *bas1* *Spo11*-oligo maps correlated moderately with the published microarray maps (Mieczkowski *et al.* 2006) (Pearson's $r = 0.47$ – 0.51) but had much higher spatial and quantitative resolution (Figure 1E). The high-resolution maps allowed us to analyze DSB activity at the individual hotspot level, which was not possible with the earlier datasets. First, we examined *Spo11*-oligo counts in mutants compared with wild type. Most hotspots were affected little if at all in the mutants (Figure 2, A and B), but a small number were increased or decreased so we sought to identify all changed hotspots. To minimize impact of experimental variation on calculated fold change of weak hotspots, only hotspots with >100 RPM in at least one map were analyzed (100 RPM is equivalent to a DSB frequency of $\sim 0.16\%$ of total DNA). After this filtering of weak hotspots, 2485 hotspots remained. We defined altered hotspots as having >20% change in *Spo11*-oligo counts with a P -value <0.1 (Student's t -test across all biological replicates, without adjustment for multiple correction).

Even with these very nonstringent criteria, only a small fraction of hotspots were detectably altered by the *bas1* mutation: 239 (9.6%) hotspots were decreased, and 87 (3.5%) were increased (Figure 2C). Of these, only 18 hotspots had changed by more than 2-fold (10 down and 8 up) (Table S3). The most decreased hotspot was in the *ADE17* promoter (17% of wild type) and the most increased was a relatively weak hotspot inside the *ADE4* open reading frame (6.1-fold higher than wild type; a stronger hotspot in the *ADE4* promoter was decreased 2.0-fold). Only 7 of the altered hotspots are in regions where the prior microarray study by Mieczkowski *et al.* (2006) also detected changes in *bas1* (at *HIS4*, *SHM2*, *GCV2*, *ADE1*, *AIM9*, *PLP2* and *YER091C-A*). Regions that did not show agreement between the studies are likely attributable to strain differences (including use of the *rad50S* mutation in prior work) and/or the low sensitivity and spatial resolution of the prior study, which did not allow precise determination of hotspot locations.

The *ino4* mutation affected more hotspots: 415 (16.7%) were decreased by >20% and 322 (13.0%) were increased (Figure 2D). Of these, 79 had changed by more than two-fold (47 down and 32 up) (Table S3). The range of hotspot activity changes in *ino4* relative to wild type was 0.23 (*OPI3-MOG1* hotspot) to 4.4 (*INO1* hotspot). Thus, deletion of these TFs is capable of changing hotspot activity, but affects only a small portion of total hotspots.

To validate results from *Spo11*-oligo mapping, we analyzed meiotic DNA formation directly by standard Southern blot analysis for hotspots at the promoters of *SHM2*, *GAT2-GID8*, *GCV2*, *CHO2*, *ADO1-SOD1*, and *FAS1* in the *rad50S*-like (DSB repair deficient) mutant *sae2*. Consistent with *Spo11*-oligo maps, DSB activity was significantly reduced for *SHM2* and elevated for *GCV2* in the *bas1* mutant (Figure 2, E–H), in agreement with previous results in a different strain background (Mieczkowski *et al.* 2006). In *ino4*, *CHO2* showed decreased DSB formation and *FAS1* showed increased DSB levels as well as altered spatial pattern (Figure 2, I–L). *GAT2-GID8* and *ADO1-SOD1* were unchanged in TF-mutant *Spo11*-oligo maps, but both hotspots were slightly increased by Southern blot analysis (Figure 2, M and N). It is important to note that *sae2* mutants suppress late-forming DSBs (Borde *et al.* 2000). The discrepancies may arise from the use of a *rad50S*-like mutant background for the Southern blot determinations or may trace to measurement imprecision in either *Spo11*-oligo maps or Southern blot determinations. Prior studies in *S. cerevisiae* and *S. pombe* have established excellent overall quantitative agreement between *Spo11* (Rec12) oligo counts and DSB frequencies measured by Southern blotting, but small differences between the methods have been noted in the past for some hotspots (Pan *et al.* 2011; Sasaki *et al.* 2013; Fowler *et al.* 2014), comparable to the differences seen here. Thus, as expected, the *Spo11*-oligo maps in general showed excellent quantitative agreement with direct assays of DSBs and, equally important, provided excellent spatial accuracy in defining DSB positions (Pan *et al.* 2011; Fowler *et al.* 2014).

Identification of *Bas1* and *Ino4* binding sites in meiotic cells

To evaluate whether hotspots altered in *bas1* or *ino4* mutants might be directly influenced by the TFs, we mapped *Bas1* and *Ino4* binding sites during meiosis by ChIP of Myc-tagged *Bas1* and *Ino4* followed by high-throughput sequencing. ChIP peaks were called as described (Murakami and Keeney 2014) (*Materials and Methods*), identifying 36 *Bas1* binding peaks and 197 *Ino4* binding peaks (Figure 3, A and B; Table S4 and Table S5). Most of these peaks (30 of the 36 *Bas1* binding peaks and 176 of the 197 *Ino4* binding peaks) were located in or near the promoters of genes. Specific enrichment of *Bas1* at the promoters of *GCV2* and *GCV3* and of *Ino4* at the *FAS2* promoter was also observed by ChIP followed by qPCR, validating results from ChIP-seq (Figure 3C).

We searched for likely TF recognition motifs in the 500 bp encompassing each ChIP-seq peak (Bailey *et al.* 2009). This

analysis identified a motif containing the core sequence 5'-GAGTCA for *Bas1* binding peaks (Figure 3D), in agreement with previous studies (Daignan-Fornier and Fink 1992; Mieczkowski *et al.* 2006; Zhu *et al.* 2009). More than half of the *Bas1* ChIP-seq peak regions (21 of 36) contained one or more match to this motif. Peaks without a match to the motif may contain degenerate *Bas1* binding sequences, may be targeted by *Bas1* via interactions with other proteins, or may be false positives from the ChIP-seq. The *Bas1* ChIP-seq peaks accounted for most (27 of 37; 70% within 500 bp) of a previously annotated set of *Bas1* binding sites (MacIsaac *et al.* 2006).

Mieczkowski *et al.* (2006) identified 56 promoter intergenic regions with ChIP evidence for binding by *Bas1* in meiotic cells and with a perfect match to the *Bas1* recognition motif. Twenty-one of these regions overlapped with our *Bas1* ChIP-seq peaks (Table S4). These overlapping *Bas1* binding sites are in the promoters of many known *Bas1*-regulated genes involved in the adenine and histidine biosynthetic pathways (*ADE1*, *ADE2*, *ADE4*, *ADE6*, *ADE8*, *ADE17*, and *HIS1*) and in one-carbon metabolism (*GCV1*, *GCV2*, *GCV3*, *MDT1*, and *SHM2*) (Denis *et al.* 1998; Denis and Daignan-Fornier 1998; Gelling *et al.* 2004). However, *HIS4* and a few other known *Bas1* targets were not identified in our dataset. For *HIS4*, a very weak ChIP-seq signal was present below the peak-calling threshold (Figure S1), presumably reflecting a quantitative difference in *Bas1* occupancy of the *HIS4* promoter between SK1 (where *HIS4* is only a modest DSB hotspot (Table S3) and the strain background used by Petes and colleagues (Stapleton and Petes 1991; Mieczkowski *et al.* 2006).

For *Ino4*, MEME identified the motif 5'-GCATGTGAAAA (Figure 3D), which matches well the upstream activation sequence recognized by *Ino2/4* (UAS_{ino}, C/AATGTGAAAT) (Bachhawat *et al.* 1995). Most (162 of 197) *Ino4* ChIP-seq peaks contained at least one match to the identified motif. Furthermore, *Ino4* ChIP-seq peaks accounted for all but one of the small number of previously annotated *Ino4* motifs (21 of 22; 95.5%) (MacIsaac *et al.* 2006).

Hotspots containing *Bas1* and *Ino4* binding sites

In a prior study using a compilation of TF binding sites by MacIsaac *et al.* (2006), we observed that 32 of 37 annotated *Bas1* sites were contained within 18 hotspots, three-fourths of which were among the hottest 50% of all hotspots (Pan *et al.* 2011). For *Ino4*, all but 1 of the 22 annotated binding sites were inside 17 hotspots, nearly all of which were among the hottest 50% of all hotspots (Pan *et al.* 2011). These findings suggested that presence of a potential binding site(s) for *Bas1* or especially *Ino4* was a good predictor of strong local DSB activity. Superficially at least, these findings also seemed to support the hypothesis that simple sequence motifs targeted by these TFs are a dominant factor shaping local DSB patterns (Wahls and Davidson 2010). However, the available TF binding site data were incomplete and did not represent DNA binding in meiotic cells. Specifically, the sites compiled

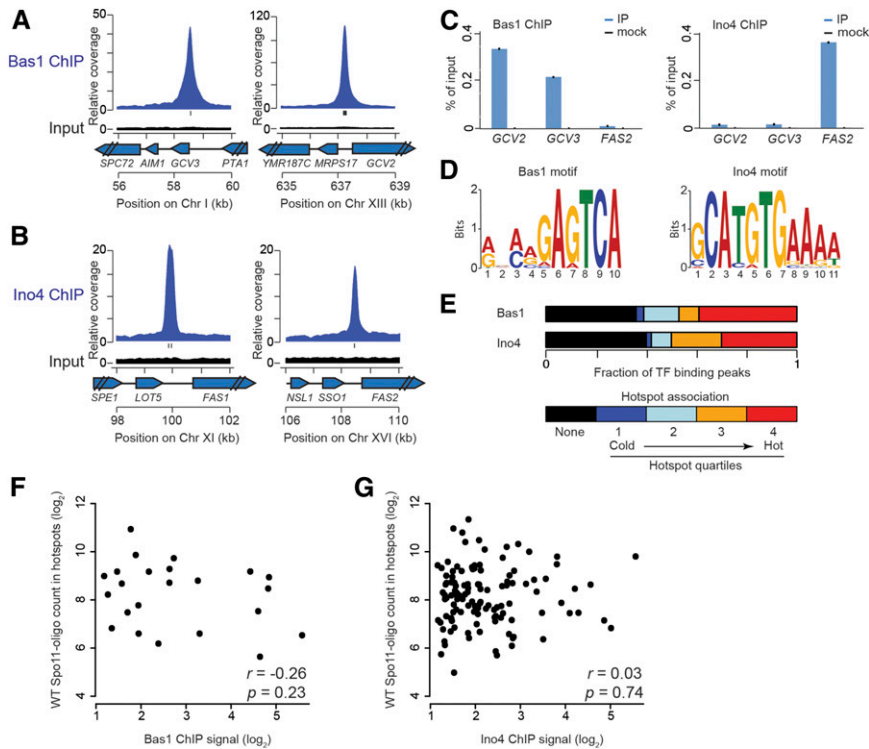


Figure 3 TF binding sites and their association with DSB hotspots in meiosis. (A and B) Examples of Bas1 (A) or Ino4 (B) ChIP-seq data. Plots show the sequence coverage relative to genome average for ChIP and input samples. Each input is plotted on the same scale as the respective ChIP data. Tick marks under the ChIP plots indicate matches to Bas1 or Ino4 motifs. (C) ChIP-qPCR at *GCV2*, *GCV3*, and *FAS2* promoters. (D) Consensus Bas1 and Ino4 motifs identified in meiotic ChIP-seq datasets. (E) Association of TF binding peaks with hotspots. Bars depict the fraction of ChIP-seq peaks not in DSB hotspots (black) and divide the remainder according to hotspot quartile. (F and G) For hotspots overlapping TF binding sites, there is no correlation between DSB hotspot activity in wild type (WT) and TF ChIP-seq signal (summed in a 401-bp window around the ChIP-seq midpoint).

by MacIsaac *et al.* (2006) marked only a minority of the ChIP-seq peaks (38.9% of *Bas1* peaks; 8.5% for *Ino4*). We therefore revisited comparisons between TF binding and DSBs with the new TF binding site data in hand.

We divided hotspots into quartiles according to *Spo11*-oligo counts and calculated the percentage of TF ChIP-seq peaks that overlapped hotspots in each quartile. Unexpectedly, ~40% of each TF's ChIP-seq peaks were in loci that did not score as hotspots, even with our nonstringent hotspot definition (Figure 3E). Thus, binding of neither *Bas1* nor *Ino4* is sufficient for high local DSB activity. Interestingly, however, those *Ino4* sites that were in hotspots tended to be in relatively hot ones, similar to our prior findings (Figure 3E). TFs bind to their target sites with different fractional occupancies *in vivo*, and the range of ChIP-seq peak intensities was large (Table S4 and Table S5), so we asked whether DSB hotspot activity correlates with TF binding strength (ChIP signal). No significant correlation was observed (Figure 3, F and G). Therefore, counter to expectation from our prior study, the binding of these TFs has essentially no predictive power for DSB activity.

Despite this lack of predictive power overall, we asked whether *Bas1* or *Ino4* influences the activity of the subset of hotspots that is directly bound by these TFs during meiosis. We used the same nonstringent criteria for defining hotspot changes as above ($P < 0.1$; >20% change from wild type; only hotspots with >100 RPM in at least one dataset). In *bas1* mutants, about half of the 23 hotspots overlapping *Bas1* ChIP-seq peaks had altered *Spo11*-oligo counts: 9 were decreased, 3 were increased (Figure 4A). Although only

a fraction, this number (12/23) is significantly higher than expected by chance ($P < 9.9 \times 10^{-6}$, Fisher's exact test comparing to the fraction (~13%) of total hotspots changed in the *bas1* mutant) (Figure 2C). In *ino4* mutants, only one-third of the 119 hotspots overlapping *Ino4* peaks were changed: 23 had decreased *Spo11*-oligo counts and 15 were increased (Figure 4B; compare to Figure 2D). This number (38/119) is no different than expectation from random (29.7% of hotspots were changed in the *ino4* mutant) ($P = 0.61$).

We further evaluated the effects of the TF mutations on local DSB activity by examining DSB changes in the TF mutants around all *Ino4* and *Bas1* binding peaks, regardless of whether these loci scored as DSB hotspots. We divided TF binding peaks into three groups according to their ChIP-seq signals, and then measured the absolute fold change in local *Spo11*-oligo counts in the TF mutants (*i.e.*, considering all changes equivalently, whether increasing or decreasing). Relative to control loci, *Bas1* binding peaks tended to show greater change in local *Spo11*-oligo density in the *bas1* mutant, and this trend was statistically significant for the two-thirds of binding peaks with the highest ChIP-seq signal (Figure 4C). No such trend was observed for *Ino4* (Figure 4D).

These findings agree with and substantially extend prior results implying that *Bas1* often influences DSB formation nearby, but that the magnitude and direction (increasing or decreasing) of influence is context dependent (Mieczkowski *et al.* 2006). In interesting contrast to *Bas1*, even though *ino4* mutation has a larger net effect on DSB distribution genome-wide, *Ino4* modulates DSB formation near its binding sites

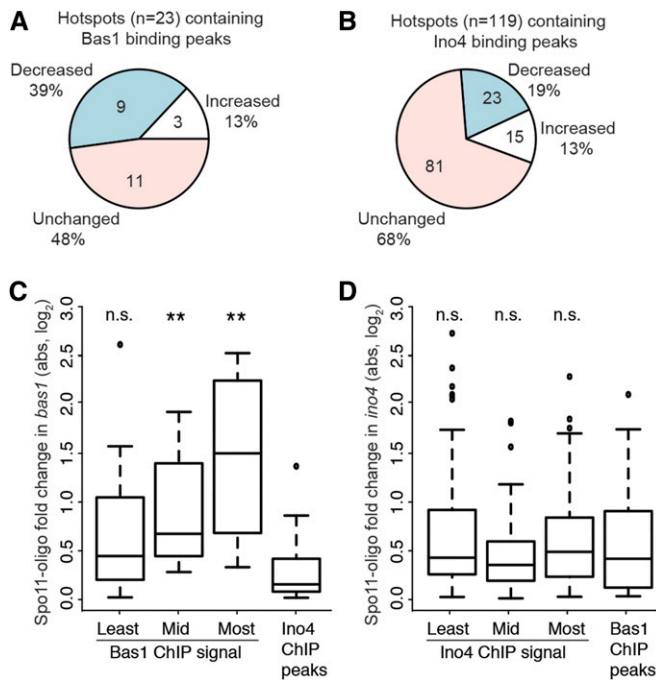


Figure 4 Context-dependent effects of *bas1* and *ino4* mutations around TF binding sites. (A and B) Proportion of hotspots overlapping TF ChIP-seq peaks that displayed at least 20% change in Spo11-oligo counts relative to wild type. (C and D) Changes in Spo11-oligo counts around all TF binding sites in the TF mutants. For each TF, all detected binding sites (regardless of whether the site was scored as a hotspot) were divided into three groups according to ChIP-seq signal, and Spo11-oligo counts were summed in 401-bp windows surrounding the peaks. Absolute log fold changes relative to wild type are plotted. Boxes indicate median and interquartile range; whiskers indicate the most extreme data points, which are ≤ 1.5 times the interquartile range from the box; individual points are outliers. For the *bas1* mutant (C), 12 Ino4 ChIP-seq peaks were randomly chosen to serve as a negative control set. For the *ino4* mutant (D), all Bas1 ChIP-seq peaks were used as the negative control. Results are shown for Wilcoxon rank-sum tests comparing each TF binding site group to the respective negative control group (n.s., not significant; $**P < 0.01$).

only rarely and thus appears to exert more of its influence indirectly. Thus, the previously apparent correlation of Ino4 binding sites with strong DSB hotspots (Pan *et al.* 2011) was not predictive of a widespread functional relationship.

Chromatin structure in and near hotspots in *bas1* and *ino4* mutants

Open chromatin structure provides a window of opportunity for Spo11 (Ohta *et al.* 1994; Wu and Lichten 1994; Fan and Petes 1996; Keeney and Kleckner 1996; Berchowitz *et al.* 2009; Pan *et al.* 2011). Given precedents of *HIS4* and *PHO5* (Introduction), a simple prediction might be that hotspots whose DSB activity is affected in TF mutants would display correlated changes in chromatin structure: increased accessibility if TF removal increases DSBs, and decreased accessibility in hotspots with decreased DSBs (Mieczkowski *et al.* 2006). We tested this prediction by examining chromatin structure in the hotspots validated by Southern blotting (Figure 2).

As described below, the relationship between chromatin and DSB changes is context specific and more complex than the simplest model would predict.

Intact nuclei were prepared from meiotic cultures of wild-type and mutant cells and partially digested with MNase. DNA was then purified and analyzed by Southern blotting (Figure 5). MNase-digested naked DNA verified that banding patterns were chromatin dependent. Genomic DNA from meiotic cultures of *sae2* mutants was run in parallel to mark the positions of meiotic DSBs.

In wild-type cells, the *SHM2* promoter (where *bas1* mutation reduces DSB formation) (Figure 2, E and G) displayed a broad zone of MNase hypersensitivity encompassing the Bas1 binding motifs, and DSBs formed across part of this zone (Figure 5A). The DSB distribution did not match the fine-scale MNase pattern, analogous to observations at *HIS4* (Fan *et al.* 1995). In the *bas1* mutant, the Bas1 motifs became strongly protected from MNase, indicating presence of a nucleosome. The remaining DSBs were now restricted to a smaller region corresponding to an MNase-hypersensitive site flanking the new positioned nucleosome (Figure 5A). Narrowing of the DSB zone was also seen in the Spo11-oligo map (Figure 2E). Previous studies showed that mutating these Bas1 motifs diminishes DSB formation in strains expressing Bas1 (Mieczkowski *et al.* 2006), so the chromatin changes we observed are presumably direct effects of Bas1.

In broad strokes, the parallel changes in chromatin and DSB formation near the Bas1 binding sites appeared similar to those at *HIS4* and *PHO5* and seemed consistent with the interpretation that reducing DNA accessibility via placement of a nucleosome may be sufficient by itself to reduce and spatially constrain DSB formation. However, the *bas1* mutant displayed substantial alteration in chromatin structure beyond the immediate vicinity of the Bas1 motifs, corresponding to reduced transcription of *SHM2* (based on RNA-seq results, discussed further below). The *SHM2* transcription unit showed a nucleosomal ladder that was broad and shallow in wild type, indicating variable nucleosome positioning in the population. This ladder was more pronounced in *bas1*, indicating a more regularly positioned array (Figure 5A). The neighboring gene (*REX2*) also had a more regular nucleosome array at its 3' end when Bas1 was absent. Furthermore, the *bas1* mutant retained just as much MNase hypersensitivity as wild type right where the residual DSB formation occurred (Figure 5A), indicating that most cells still present a usable window of opportunity for Spo11. Because the *bas1* mutant still has accessible DNA that can be targeted for DSB formation, and because absence of Bas1 triggers chromatin restructuring several kilobases around this locus, it is possible that the change in DSB frequency is caused by other factors besides a change in nucleosome occupancy at the positions where Spo11 cleaves (addressed further in Discussion).

Substantial chromatin changes were also observed in the *GCV2-MRPS17* intergenic region, which experiences more

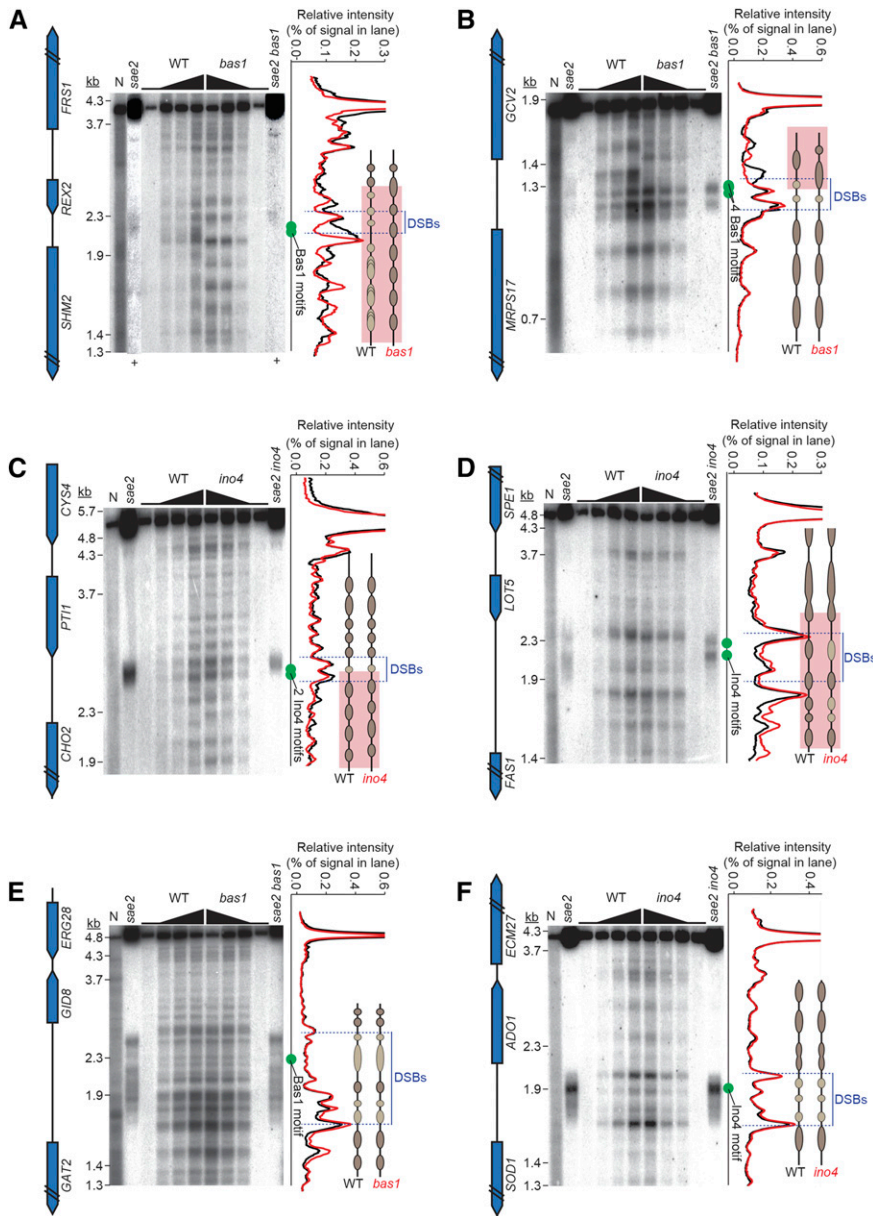


Figure 5 Chromatin structure in and around hotspots in wild type and TF mutants. MNase digestion patterns are shown for *SHM2* (A), *GCV2* (B), *CHO2* (C), *FAST* (D), *GAT2-GID8* (E), and *ADO1-SOD1* (F). Intact meiotic nuclei were treated with zero or increasing amounts of MNase, and then DNA was purified, digested with restriction enzymes, and analyzed by Southern blotting and indirect end labeling. DSB positions are shown using DNA purified from *sae2* meiotic cultures. N, naked DNA (purified genomic DNA from vegetative cells, treated with MNase). Approximate positions of Bas1 or Ino4 motifs are indicated with green dots. The hybridization signals from the lanes with highest MNase concentration are plotted on the right of each panel, with interpretive cartoons illustrating regions of MNase resistance: darker brown ovals for regions that are relatively more MNase-resistant, lighter tan ovals for relatively less resistant, black lines for MNase-hypersensitive, and pink highlighting for regions with changed MNase digestion patterns. Note that the ovals do not necessarily correspond to positioned nucleosomes; some are smaller than nucleosomes and may reflect footprints of transcription factors and/or subnucleosomal histone particles. + signs in A indicate lanes for which contrast was separately enhanced to show the DSB positions better.

DSBs in *bas1*. Wild-type cells displayed a broad MNase-hypersensitive site near the 5' end of *GCV2* (Figure 5B). This site was flanked on the *GCV2*-proximal side by a zone of protection, presumably from a well-positioned, high-occupancy nucleosome overlapping the 5' end of *GCV2*. On the *GCV2*-distal side, two more strong MNase-hypersensitive sites were interdigitated with two areas of modest protection smaller than nucleosomes, presumably from subnucleosomal histone particles or other DNA binding proteins. One of the strong MNase sites overlapped four closely spaced Bas1 motifs. A nucleosome ladder extended into the adjacent *MRPS17* gene, which is expressed during sporulation and is not regulated by Bas1 (see below). DSBs occurred diffusely throughout a region encompassing the *MRPS17*-proximal MNase-hypersensitive sites and trailing weakly into the hypersensitive site that overlapped most of the Bas1 motifs. As

at *SHM2*, DSBs correlated little with the fine-scale MNase pattern (Figure 5B).

In *bas1*, the broad MNase-hypersensitive site nearest to *GCV2* disappeared; apparently the nucleosome that should overlap the 5' end of *GCV2* was now positioned over this region (Figure 5B). The nucleosome array over the *GCV2* transcription unit was also repositioned and less distinct. In contrast, the nucleosome ladder in *MRPS17* and the MNase-hypersensitive sites closer to *MRPS17*—including the one overlapping the Bas1 motifs—were unaffected. Meiotic DSBs not only became more frequent, they were now more spatially restricted and more closely followed the pattern of MNase cleavage, including prominent cleavage overlapping the Bas1 motifs (Figure 2F and Figure 5B).

A straightforward interpretation is that DSBs in wild type occur in portions of the adjacent *MRPS17* and *GCV2*

promoters. Absent *Bas1*, part of the *GCV2* promoter becomes occluded by a nucleosome that partially blocks *Spo11* access. Nonetheless, hotspot activity increases, with *Spo11* now more constrained to cleave within a pair of MNase-hypersensitive sites closer to the *MRPS17* promoter. Note that, while this intergenic region became more MNase resistant overall, accessibility of the *MRPS17*-proximal MNase-hypersensitive sites themselves did not detectably change. Thus, the fine-scale DSB distribution within the hotspot reflects DNA accessibility changes, but quantitative measures of MNase accessibility are a poor predictor of total DSB levels.

The *CHO2* promoter contains two *Ino4* motifs and experiences a decrease in DSBs in the *ino4* mutant (Figure 2, I and K). In wild type, a pair of strong MNase-hypersensitive sites bracketed a subnucleosomal-sized zone of modest protection overlapping the motifs (Figure 5C). Positioned nucleosomes were present across the *CHO2* transcription unit and the 3' end of the adjacent gene (*PTI1*). DSBs were concentrated across the MNase-hypersensitive sites around the *Ino4* motifs, including the motifs themselves and their small MNase-protected zone (Figure 2I and Figure 5C). The *ino4* mutant had a small decrease in MNase cleavage in the more *CHO2* proximal of the pair of MNase-hypersensitive sites near the motifs, but this segment overall remained strongly MNase hypersensitive (Figure 5C). There was a pronounced change in the spacing of nucleosomes across the *CHO2* transcription unit, but no changes were seen upstream of the *Ino4* motifs across *PTI1*. DSBs had similar spatial patterning in the TF mutant as in wild type, agreeing with the *Spo11*-oligo maps (Figure 2I and Figure 5C). Thus, the essentially unchanged chromatin accessibility right at the DSB hotspot paralleled the relatively unchanged DSB distribution, whereas the number of DSBs and the chromatin structure in the adjacent transcription unit changed substantially.

The *FAS1* promoter also contains two *Ino4* motifs, but this region experiences an increase in DSB formation in *ino4* (Figure 2, J and L). In wild type, two strong MNase-hypersensitive sites were located on either side of a more modest doublet of MNase sensitivity, with the *Ino4* motifs in a more MNase-resistant portion of this segment (Figure 5D). DSBs formed a pair of smears across the region containing the *Ino4* motifs and bore little similarity to the fine-scale MNase pattern. In the *ino4* mutant, much of the intergenic region became modestly more sensitive to digestion, but the spatial array of bands was not detectably altered and the strong MNase-hypersensitive sites were largely unchanged (Figure 5D). DSBs were spread across a similar total area as in wild type, but redistributed so that segments containing the *Ino4* motifs received a higher fraction of total DSBs. In this case, increased DSB frequency correlated with increased overall MNase hypersensitivity.

Finally, as controls we examined the *GAT2–GID8* and *SOD1–ADO1* intergenic regions, which contain single *Bas1* or *Ino4* motifs, respectively, and whose DSB levels were unchanged in the TF mutants (Figure 2, M and N). *GAT2–GID8* displayed a complex MNase pattern, with numerous MNase-hypersensitive

sites upstream of the 5' end of *GAT2* and a smaller hypersensitive zone near the 5' end of *GID8* (Figure 5E). DSBs were distributed across much of the intergenic region, and again the DSB spatial pattern correlated poorly with the fine-scale MNase pattern. Absence of *Bas1* caused little or no change in the MNase pattern, even around the *Bas1* motif, and there was likewise little change in the DSB pattern (Figure 5E). Similarly, *SOD1–ADO1* displayed several MNase hypersensitive sites spanning the region where DSBs appeared as a diffuse smear, with no clear correlation of DSBs with MNase cleavage (Figure 5F). We observed no change in either chromatin structure or DSB distribution in the *ino4* mutant.

Taken together, these examples show that the relationships between TF binding, local chromatin structure, and DSB patterns are complex and context specific. In three cases where removing the TF affected chromatin structure right where DSBs would normally form, we observed corresponding changes in the fine-scale DSB distribution (Figure 5, A, B, and D). Conversely, fine-scale DSB patterns were not altered at three loci with unchanged MNase patterns around the wild-type DSB positions (Figure 5, C, E, and F). Importantly, however, there was no clear correlation between quantitative changes in MNase sensitivity and changes in overall DSB frequencies, ruling out effects on chromatin accessibility alone as a universal explanation for how TFs modulate DSB hotspot activity.

Changes in DSB frequency do not correlate with changes in histone H3 lysine 4 trimethylation around hotspots

In meiosis, sister chromatids form a linear protein axis (the axial element), with chromatin emanating out in loops; DSBs are more likely to occur in DNA sequences that are in loops, but many of the proteins needed for DSB formation are enriched on the axis (Blat *et al.* 2002; Kumar *et al.* 2010; Panizza *et al.* 2011). This and other observations have led to a “tethered loop–axis complex” model in which DSBs are formed in loop segments captured by axis-associated DSB machinery (Blat *et al.* 2002; Panizza *et al.* 2011) (Figure 6A). Recently, it was discovered that the DSB-promoting protein *Mer2* interacts with *Spp1*, a protein containing a PHD (Plant Homeo Domain) finger that binds H3K4me3 marks and may thereby tether the chromatin loop to the axis, promoting DSB formation in nucleosome-depleted regions in loops (Acquaviva *et al.* 2013; Sommermeyer *et al.* 2013). Thus, one hypothesis to account for altered DSB frequencies could be that deletion of TFs alters the H3K4me3 modification status around certain promoters and thereby affects *Spp1*-dependent targeting efficiency.

To test this hypothesis, we performed ChIP-seq to measure H3K4me3 levels in wild type and TF mutants. Cells from 4-hr meiotic cultures were crosslinked with formaldehyde and disrupted. Chromatin was digested into mononucleosomes with MNase, immunoprecipitated with antihistone H3 and anti-H3K4me3 antibodies, and deep sequenced. Resulting maps showed the expected pattern of preferential H3K4me3 enrichment for nucleosomes

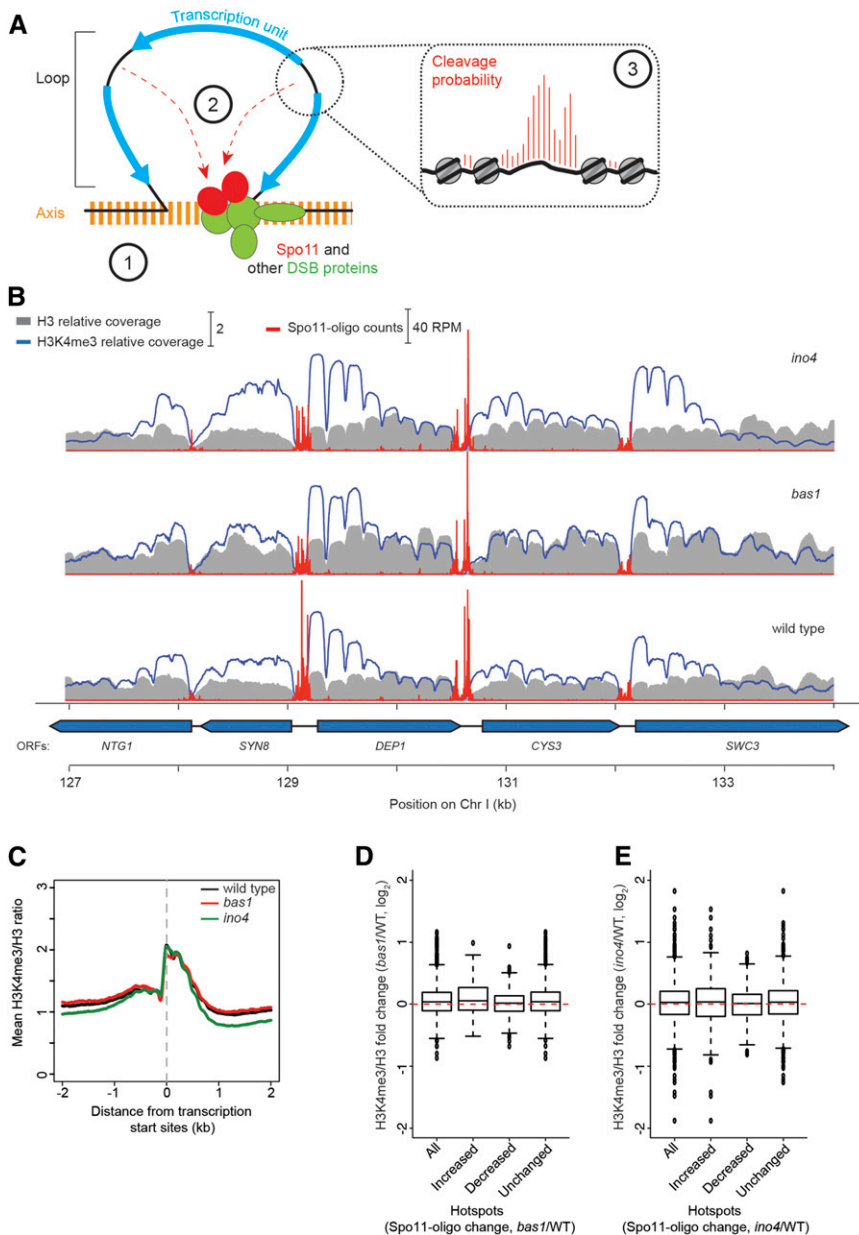


Figure 6 Tethered loop-axis model for DSB formation, and H3K4me3 levels in *bas1* and *ino4* mutants. (A) Tethered loop-axis model for DSB formation (based on Blat *et al.* 2002; Panizza *et al.* 2011; Acquaviva *et al.* 2013; Sommermeyer *et al.* 2013). Encircled numerals highlight potentially TF-dependent levels of the hierarchical combination of factors that shape the DSB distribution. (1) DSB-forming potential over regions of ~5–20 kb is established by the loop-axis structure of meiotic chromosomes and the axis-association of DSB-promoting proteins. (2) Within a loop, gene promoters are preferentially targeted for DSB formation, in part by interactions between the DSB machinery and promoter-proximal H3K4me3. (3) Within a hotspot, the fine-scale distribution of DSBs is shaped in part by accessibility of the DNA to Spo11, in competition with nucleosomes and other DNA binding proteins. (B) Snapshot of anti-H3K4me3 and anti-H3 ChIP-seq data from wild-type, *bas1*, and *ino4* datasets. Sequence coverage values are normalized to genome average. Spo11-oligo counts are superimposed for comparison. (C) Average profiles of H3K4me3/H3 ratios relative to transcription start sites. (D and E) Log fold change of H3K4me3/H3 ratios in groups of hotspots that responded as indicated to the *bas1* (D) or *ino4* (E) mutations. Hotspot groups are as indicated in Figure 2, C and D. Because the hotspots themselves are highly nucleosome depleted, we summed H3K4me3/H3 ratios in 500-bp windows offset by 200 bp away to the left and right of each hotspot's midpoints.

near the 5' ends of most genes (Figure 6, B and C) (Pokholok *et al.* 2005; Borde *et al.* 2009; Zhang *et al.* 2011b). However, counter to the hypothesis motivating this analysis, we observed no significant difference between the increased, decreased, and unchanged DSB hotspot groups when we examined the change in H3K4me3-to-H3 ratios caused by the *bas1* or *ino4* mutation (Figure 6, D and E). Thus, changes in the level of this histone modification in TF mutants provide no predictive power for changes in DSB frequency. This finding fits with the observation that, even though H3K4me3 promotes Spo11 activity in most promoter regions (84% of DSB sites exhibited a severely reduced DSB frequency in the absence of H3K4me3) (Borde *et al.* 2009; Acquaviva *et al.* 2013; Sommermeyer *et al.* 2013), quantitative measures of H3K4me3 correlate poorly if at all with DSB hotspot strength (Tischfield and Keeney 2012).

Changes in DSB frequencies do not correlate with changes in gene expression

Mutation of the TATA box at *HIS4* greatly reduces transcription with little effect on DSB frequency, so transcription is not required for hotspot activity of a promoter (White *et al.* 1992). Furthermore, genome-wide correlations between transcription activity and DSB frequencies in promoters are weak to nonexistent (Tischfield and Keeney 2012). Nonetheless, to address the possibility that changes in hotspot activity in TF mutants might reflect alterations in transcription, RNA-seq was carried out during meiosis in wild-type, *bas1*, and *ino4* strains (Figure 7, A and B). We identified 222 significantly up-regulated and 341 down-regulated genes in *bas1* mutants, as well as 27 up-regulated and 112 down-regulated

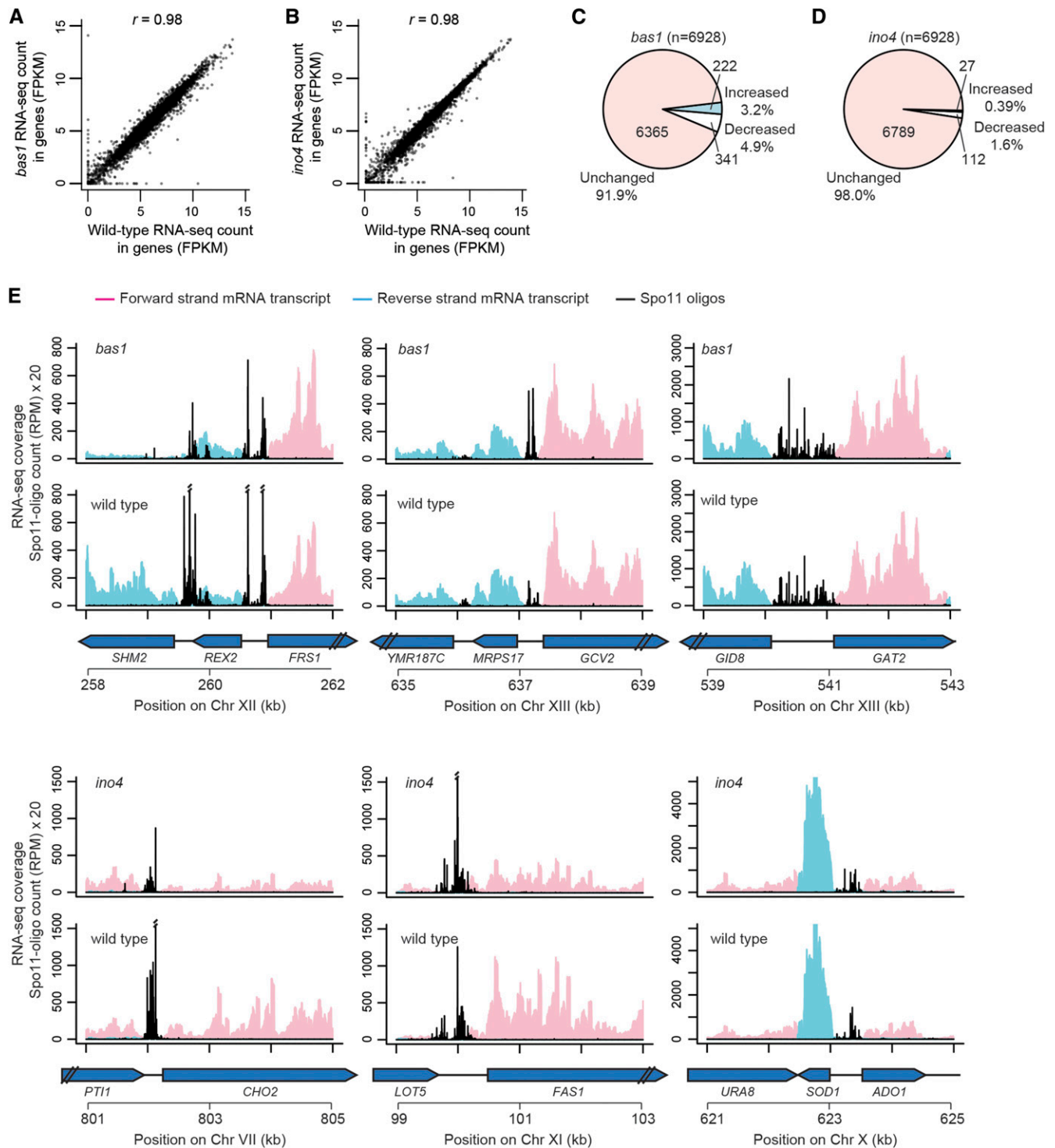


Figure 7 mRNA levels in *bas1* and *ino4* mutants. (A and B) Comparisons of RNA-seq read counts (in fragments per kilobase per million mapped reads, FPKM, log₂-transformed) between wild type and TF mutants for all annotated genes. (C and D) Proportion of genes that were significantly changed relative to wild type (false discovery rate $q < 0.05$). (E) Snapshots of RNA-seq data around hotspots at the promoters of *SHM2*, *GCV2*, *GAT2-GID8*, *CHO2*, *FAS1*, and *ADO1-SOD1*. Per-base pair RNA-seq coverage is plotted separately for forward and reverse reads after normalization to set the total coverage as equal in all samples. The profile for each genotype is the average of the normalized coverage maps from two biological replicates. Double slashes indicate where Spo11-oligo counts are off scale.

genes in *ino4* mutants (false discovery rate $q < 0.05$) (Figure 7, C and D; Table S6 and Table S7). Bas1-regulated genes were enriched for Gene Ontology (GO) terms purine nucleotide metabolic process (31 of 563 genes, 5.5%), phosphorus

metabolic process (93 genes, 16.5%), carboxylic acid metabolic process (56 genes, 9.9%), and meiotic cell cycle process (68 genes, 12.1%). Ino4-regulated genes were enriched for GO terms lipid biosynthetic process (13 of 139 genes, 9.4%)

and meiotic cell cycle process (25 genes, 18.0%). Thus, in addition to known Bas1- or Ino4-regulated pathways, some genes involved in meiosis were also differentially expressed in *bas1* and *ino4*. This may reflect direct or indirect effects of these TF mutations on meiotic entry or progression or genotype-independent differences from culture-to-culture variation in timing.

Next, we examined the gene expression patterns around the six hotspots characterized above. Each of these hotspots contained a Bas1 or Ino4 ChIP-seq peak, but TF deletion had different effects on gene expression. As expected (Denis and Daignan-Fornier 1998), *SHM2* mRNA level was substantially reduced (8.9-fold) after deleting Bas1 (Figure 7E; Table S6). In contrast, mRNA levels of *GCV2* and *MRPS17* were unchanged in *bas1*, even though the chromatin structure at *GCV2* was substantially altered (Figure 5B) and DSB frequency in this divergent intergenic region was increased. For Ino4-bound hotspots, both *CHO2* and *FAS1* showed similarly reduced mRNA levels in *ino4* (3.3- and 2.5-fold, respectively) (Figure 7E; Table S7), but had DSB levels that moved in opposite directions. For the genes flanking the control (unchanged) hotspots *GID8-GAT2* and *ADO1-SOD1*, mRNA levels were unchanged in the TF mutants. Thus, there is no simple correlation between changes in Spo11-oligo counts and mRNA levels.

To extend this analysis to the whole genome, we plotted the fold change of mRNA level for each nondubious gene against the fold change of Spo11-oligo counts in its promoter (Figure 8). Both mutants showed significant but very weak correlations between these changes, such that variation in transcript levels explained $\leq 0.8\%$ of the variation in promoter DSB frequency. For several Bas1 and Ino4 targets (*SHM2*, *GCV1*, *ADE17*, and *GCV3* for Bas1 and *OPI3* for Ino4), both gene expression and hotspot activities were decreased in the respective TF mutant. However, there were numerous exceptions to this trend. For example, *GCV2* and *IRC22* showed increased promoter DSB frequency but unchanged RNA levels in *bas1*; *GNP1* behaved similarly in the *ino4* mutant. Meanwhile, expression of *INO1* in the *ino4* mutant and *YOR302W* in the *bas1* mutant was substantially reduced with little accompanying change in promoter DSB activity. Thus, changes in mRNA level in TF mutants provide little or no predictive power for changes in DSB frequency. These results strengthen and extend the conclusion from previous work (White *et al.* 1992) that DSB hotspot activity of promoters is not tied to transcriptional activity *per se*.

Discussion

DNA sequence-dependent targeting of meiotic recombination was first discovered more than two decades ago in two highly diverged organisms, fission yeast and budding yeast (Ponticelli *et al.* 1988; Schuchert *et al.* 1991; White *et al.* 1991). Additional regulatory DNA sites were identified subsequently in both yeasts (White *et al.* 1993; Fan *et al.* 1995; Steiner

et al. 2009), and more recently it was found that mouse and human hotspots are defined by the histone methyltransferase PRDM9 binding to specific DNA sequences (Baudat *et al.* 2010; Myers *et al.* 2010; Grey *et al.* 2011; Brick *et al.* 2012; Pratto *et al.* 2014). These and other findings have focused attention on the roles of sequence-specific DNA binding proteins in shaping the DSB landscape and have even led to proposals that one or a few such proteins and their binding sites are the principal architects of DSB hotspot location and activity across all of both yeasts' genomes (e.g., Wahls and Davidson 2010).

Sequence-specific DNA binding by PRDM9 is clearly a primal determinant of hotspots in most mammalian species (*Prdm9* knockout mice still have many hotspots, but at other places) (Brick *et al.* 2012). However, the situation has been less clear for TFs in yeasts. Even those sequence motifs and their binding factors that are clearly capable of specifying strong DSB hotspot activity in some genomic contexts work poorly or not at all in other contexts (Ponticelli and Smith 1992; Mieczkowski *et al.* 2006; this work). Moreover, presence of a sequence motif with DSB-targeting potential is by itself a poor predictor of local DSB frequency (Mieczkowski *et al.* 2006; Fowler *et al.* 2014).

An alternative to a DNA sequence-centric view is a model in which DSB distributions are shaped by combinatorial action of many chromosomal factors that work in a hierarchical and scale-dependent manner (Petes 2001; Mieczkowski *et al.* 2006; Lichten 2008; Lichten and de Massy 2011; Pan *et al.* 2011; de Massy 2013). In this view, individual sequence-specific DNA binding proteins may contribute significantly to the DSB landscape, but in a circumscribed and highly context-dependent manner. Our findings in this study, in agreement with earlier work by Mieczkowski *et al.* (2006), support the latter model.

Because the earlier genome-wide study of Bas1 used a low-resolution microarray and focused on information for probes corresponding to entire individual ORFs (Mieczkowski *et al.* 2006), it was difficult to assign the hybridization signal to individual DSB hotspots. Therefore, we wished to revisit this question with the higher resolution and greater dynamic range afforded by Spo11-oligo mapping. Mieczkowski *et al.* (2006) scored 153 ORFs as having statistically significantly different *rad50S* ChIP-chip signal in the *bas1* mutant (68 with decreased signal in *bas1* and 85 with increased signal). We resolved more total DSB hotspots by Spo11-oligo mapping, at least in part because we were able to more precisely localize changes in DSB formation, including fine-scale changes of local DSB distribution within hotspots that were previously impossible to discern. Importantly, however, both studies support the same general conclusion: Bas1 effects on DSB formation are highly context dependent. Our results with Ino4 were similar in this regard, suggesting that context dependence is likely to be true for many if not all TFs that impinge on Spo11 activity.

Deletion of Bas1 affected DSB activity in about half of hotspots containing Bas1 binding sites, similar to frequencies

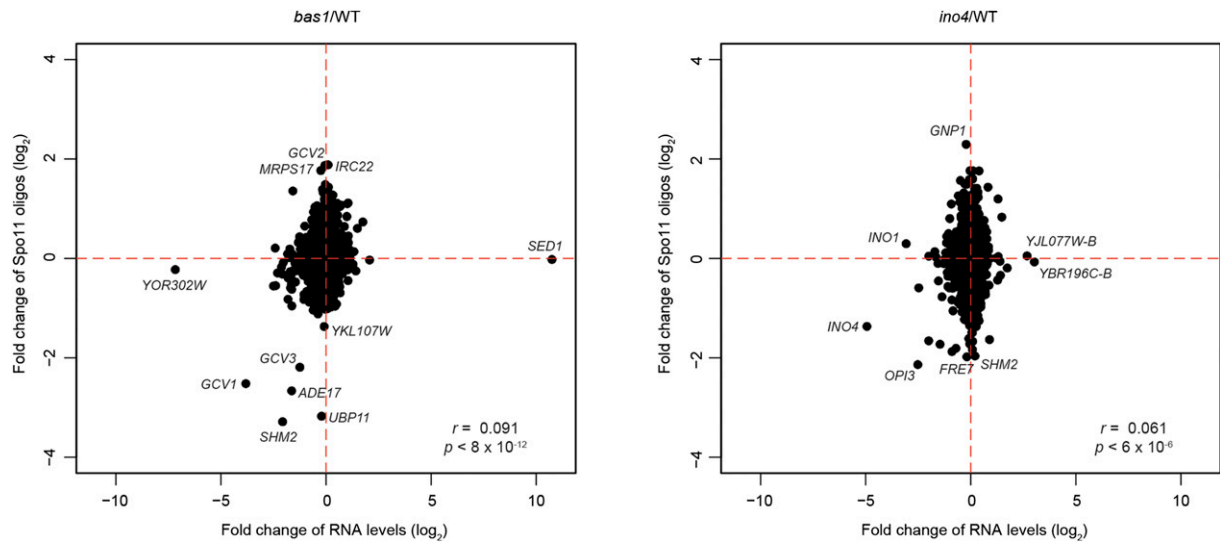


Figure 8 Comparing changes in mRNA levels with changes in promoter DSBs in *bas1* and *ino4* mutants. Spo11 oligos were summed in 300-bp windows upstream from each gene's start codon. Points corresponding to exemplar genes are labeled.

observed previously (Mieczkowski *et al.* 2006). Deletion of *Ino4* affected less than one-third of the hotspots to which *Ino4* binds directly during meiosis. Moreover, only a minority fraction of the hotspots that changed in the TF mutants were detectably bound by *Bas1* or *Ino4* protein during meiosis. This modest correspondence between TF binding and DSB activity is analogous to the relation of TFs to transcriptional regulation: numerous studies have documented that only a small fraction of genes whose promoters are bound by a given TF show expression changes when the TF is deleted, and only a small fraction of the genes that change expression are direct binding targets (reviewed in MacQuarrie *et al.* 2011; Hughes and De Boer 2013). Although it is possible that the ChIP-seq failed to detect direct *Bas1* or *Ino4* binding that does in fact occur, the results strongly indicate that a substantial portion of the DSB-modulating activity of these TFs is indirect. One possibility is that each TF mutant causes changes in cell physiology that, by crosstalk between transcriptional regulation networks, alter DSB activity at numerous gene promoters genome-wide via changes in local chromatin structure or loop-axis architecture. In this context, it is noteworthy that recombination distributions can be altered by auxotrophies for certain amino acids or nucleobases, including auxotrophies caused by mutation of several of the genes whose expression is known to be *Bas1* dependent, such as *HIS4* and *ADE1* (Abdullah and Borts 2001; Cotton *et al.* 2009). We found no correlation between DSB changes and gene expression changes in *bas1* and *ino4* mutants, but it remains possible that chromatin and higher order chromosome structure in and around the indirectly changed hotspots is affected.

In principle, indirect effects could also arise if hotspots that are direct TF targets influence neighboring hotspots via “hotspot competition.” Insertion of very strong artificial hotspots can suppress the activity of nearby hotspots over distances

up to tens of kilobases (Wu and Lichten 1995; Xu and Kleckner 1995; Fan *et al.* 1997; Ohta *et al.* 1999; Jessop *et al.* 2005). If a DSB hotspot becomes substantially hotter or colder in *bas1* or *ino4* mutants, competition could cause compensatory changes in DSB frequency in nearby hotspots. Such an effect predicts that change of a DSB hotspot in the TF mutants should be inversely correlated with changes of neighboring hotspots. However, we did not detect such a pattern in our data whether considering all hotspots relative to their neighbors or considering only the subset of direct TF targets that were most altered in the TF mutants (Figure S1, C and D). It is possible that hotspot competition is a property of artificial hotspots but not natural hotspots, but we favor instead the interpretation that the hotspots affected by *bas1* or *ino4* mutation are generally not strong enough to reveal hotspot competition in a cell population. The hottest hotspot that was directly bound by *Bas1* or *Ino4* and also showed at least a twofold change in activity had a Spo11-oligo count of only 1134 RPM (Table S3), equivalent to a DSB frequency of <2.5% of DNA according to the regression relationship in Pan *et al.* (2011), and most such hotspots had an inferred DSB frequency of <1%. For a hotspot with a DSB frequency of 2.5% of DNA, DSBs occur at this locus in $\leq 10\%$ of the cell population (assuming one DSB per four chromatids in most cells) (Zhang *et al.* 2011a). Any potential suppression by this hotspot of its neighbors would likely be masked by the behavior of the majority of unaffected cells. These considerations indicate that hotspot competition is unlikely to be a significant source of the indirect effects of TF mutations on hotspot activity.

The context dependence for *Bas1* effects on DSBs has previously been framed as reflecting locus-specific differences in the balance between chromatin “loosening” and “tightening” activities (Mieczkowski *et al.* 2006). However, for those sites

we examined directly, there was no obvious correlation between changes in DSB frequency and changes in overall MNase hypersensitivity, suggesting that chromatin accessibility is not the principal link between TFs and DSB frequency at most hotspots. In contrast, if chromatin structure immediately within a DSB hotspot was altered by TF mutation, then the fine-scale DSB pattern was also generally altered. In particular, a shift of nucleosome position or appearance of a new nucleosome at *SHM2* and *GCV2* appeared to result in local occlusion of *Spo11* access to the DNA, consistent with inferences from genome-wide studies of DSBs relative to well-positioned nucleosomes (Pan *et al.* 2011). We interpret these results to mean that open chromatin provides windows of opportunity where *Spo11* can cut, but it is not generally sufficient to determine overall break frequencies.

Interpreting our findings in the context of the tethered loop-axis complex model, we envision that regional factors (working on ~5- to 20-kb scales) shape loop-axis architecture and determine the DSB potential of a particular loop region (level 1 in Figure 6A). Within a loop, interactions between axis-bound DSB proteins and loop chromatin promotes targeting of *Spo11* activity to particular locations (*i.e.*, hotspots). These interactions determine the relative likelihood that particular hotspots will fulfill the DSB-forming potential of the loop they reside in (level 2 in Figure 6A). Within a hotspot, fine-scale DSB patterns are shaped by geometry of the targeting mechanism plus competition of *Spo11* with nucleosomes and other DNA-binding proteins (level 3 in Figure 6A). TFs can affect DSB formation at any (or all) of the levels shown; the context dependence presumably reflects differences in how a given TF influences each of these levels at various genomic regions. Thus, while there are common themes and general patterns, each hotspot tells its own story and TFs can play many and varied roles.

Acknowledgments

We thank Agnes Viale and the Memorial Sloan Kettering Cancer Center (MSKCC) Integrated Genomics Operation for DNA sequencing; Nick Socci and the MSKCC Bioinformatics Core Facility for assistance with data analysis; Stewart Shuman (MSKCC) for gifts of T4 RNA ligase; Kunihiro Ohta (Tokyo University) and Mariko Sasaki (present address: Tokyo University) for strains; Beate Schwer (Weill Cornell Medical College) for assistance with RNA-seq experiments; Cong Huang, Hajime Murakami, Jing Pan, and Jodi-Ann Sampson for experimental assistance; and members of the S.K. laboratory, especially Corentin Claeys Bouuaert, Sarah Kim, Isabel Lam, Neeman Mohibullah, Hajime Murakami, Sam Tischfield, and Shintaro Yamada, for discussion and comments on the manuscripts. This work was supported by National Institutes of Health grant R01 GM058673. S.K. is an investigator of the Howard Hughes Medical Institute.

Literature Cited

- Abdullah, M. F., and R. H. Borts, 2001 Meiotic recombination frequencies are affected by nutritional states in *Saccharomyces cerevisiae*. *Proc. Natl. Acad. Sci. USA* 98: 14524–14529.
- Acquaviva, L., L. Szekvolgyi, B. Dichtl, B. S. Dichtl, C. de La Roche Saint Andre *et al.*, 2013 The COMPASS subunit Spp1 links histone methylation to initiation of meiotic recombination. *Science* 339: 215–218.
- Alani, E., R. Padmore, and N. Kleckner, 1990 Analysis of wild-type and *rad50* mutants of yeast suggests an intimate relationship between meiotic chromosome synapsis and recombination. *Cell* 61: 419–436.
- Arndt, K. T., C. Styles, and G. R. Fink, 1987 Multiple global regulators control *HIS4* transcription in yeast. *Science* 237: 874–880.
- Bachhawat, N., Q. Ouyang, and S. A. Henry, 1995 Functional characterization of an inositol-sensitive upstream activation sequence in yeast. A cis-regulatory element responsible for inositol-choline mediated regulation of phospholipid biosynthesis. *J. Biol. Chem.* 270: 25087–25095.
- Bailey, T. L., M. Boden, F. A. Buske, M. Frith, C. E. Grant *et al.*, 2009 MEME SUITE: tools for motif discovery and searching. *Nucleic Acids Res.* 37: W202–W208.
- Baudat, F., J. Buard, C. Grey, A. Fledel-Alon, C. Ober *et al.*, 2010 PRDM9 is a major determinant of meiotic recombination hotspots in humans and mice. *Science* 327: 836–840.
- Baudat, F., and A. Nicolas, 1997 Clustering of meiotic double-strand breaks on yeast Chromosome III. *Proc. Natl. Acad. Sci. USA* 94: 5213–5218.
- Berchowitz, L. E., S. E. Hanlon, J. D. Lieb, and G. P. Copenhaver, 2009 A positive but complex association between meiotic double-strand break hotspots and open chromatin in *Saccharomyces cerevisiae*. *Genome Res.* 19: 2245–2257.
- Bergerat, A., B. de Massy, D. Gabelle, P. C. Varoutas, A. Nicolas *et al.*, 1997 An atypical topoisomerase II from Archaea with implications for meiotic recombination. *Nature* 386: 414–417.
- Blat, Y., R. U. Protacio, N. Hunter, and N. Kleckner, 2002 Physical and functional interactions among basic chromosome organizational features govern early steps of meiotic chiasma formation. *Cell* 111: 791–802.
- Blitzblau, H. G., G. W. Bell, J. Rodriguez, S. P. Bell, and A. Hochwagen, 2007 Mapping of meiotic single-stranded DNA reveals double-strand-break hotspots near centromeres and telomeres. *Curr. Biol.* 17: 2003–2012.
- Borde, V., A. S. Goldman, and M. Lichten, 2000 Direct coupling between meiotic DNA replication and recombination initiation. *Science* 290: 806–809.
- Borde, V., W. Lin, E. Novikov, J. H. Petrini, M. Lichten *et al.*, 2004 Association of Mre11p with double-strand break sites during yeast meiosis. *Mol. Cell* 13: 389–401.
- Borde, V., N. Robine, W. Lin, S. Bonfils, V. Geli *et al.*, 2009 Histone H3 lysine 4 trimethylation marks meiotic recombination initiation sites. *EMBO J.* 28: 99–111.
- Brick, K., F. Smagulova, P. Khil, R. D. Camerini-Otero, and G. V. Petukhova, 2012 Genetic recombination is directed away from functional genomic elements in mice. *Nature* 485: 642–645.
- Buhler, C., V. Borde, and M. Lichten, 2007 Mapping meiotic single-strand DNA reveals a new landscape of DNA double-strand breaks in *Saccharomyces cerevisiae*. *PLoS Biol.* 5: e324.
- Chen, S. Y., T. Tsubouchi, B. Rockmill, J. S. Sandler, D. R. Richards *et al.*, 2008 Global analysis of the meiotic crossover landscape. *Dev. Cell* 15: 401–415.
- Cotton, V. E., E. R. Hoffmann, M. F. Abdullah, and R. H. Borts, 2009 Interaction of genetic and environmental factors in *Saccharomyces cerevisiae* meiosis: the devil is in the details. *Methods Mol. Biol.* 557: 3–20.

- Daignan-Fornier, B., and G. R. Fink, 1992 Coregulation of purine and histidine biosynthesis by the transcriptional activators BAS1 and BAS2. *Proc. Natl. Acad. Sci. USA* 89: 6746–6750.
- de Massy, B., 2013 Initiation of meiotic recombination: How and where? Conservation and specificities among eukaryotes. *Annu. Rev. Genet.* 47: 563–599.
- de Massy, B., V. Rocco, and A. Nicolas, 1995 The nucleotide mapping of DNA double-strand breaks at the *CYS3* initiation site of meiotic recombination in *Saccharomyces cerevisiae*. *EMBO J.* 14: 4589–4598.
- Denis, V., and B. Daignan-Fornier, 1998 Synthesis of glutamine, glycine and 10-formyl tetrahydrofolate is coregulated with purine biosynthesis in *Saccharomyces cerevisiae*. *Mol. Gen. Genet.* 259: 246–255.
- Denis, V., H. Boucherie, C. Monribot, and B. Daignan-Fornier, 1998 Role of the myb-like protein bas1p in *Saccharomyces cerevisiae*: a proteome analysis. *Mol. Microbiol.* 30: 557–566.
- Dobin, A., C. A. Davis, F. Schlesinger, J. Drenkow, C. Zaleski *et al.*, 2013 STAR: ultrafast universal RNA-seq aligner. *Bioinformatics* 29: 15–21.
- Fan, Q., F. Xu, and T. D. Petes, 1995 Meiosis-specific double-strand DNA breaks at the *HIS4* recombination hot spot in the yeast *Saccharomyces cerevisiae*: control in *cis* and *trans*. *Mol. Cell. Biol.* 15: 1679–1688.
- Fan, Q. Q., and T. D. Petes, 1996 Relationship between nuclease-hypersensitive sites and meiotic recombination hot spot activity at the *HIS4* locus of *Saccharomyces cerevisiae*. *Mol. Cell. Biol.* 16: 2037–2043.
- Fan, Q. Q., F. Xu, M. A. White, and T. D. Petes, 1997 Competition between adjacent meiotic recombination hotspots in the yeast *Saccharomyces cerevisiae*. *Genetics* 145: 661–670.
- Fowler, K. R., M. Sasaki, N. Milman, S. Keeney, and G. R. Smith, 2014 Evolutionarily diverse determinants of meiotic DNA break and recombination landscapes across the genome. *Genome Res.* 24: 1650–1664.
- Gelling, C. L., M. D. Piper, S. P. Hong, G. D. Kornfeld, and I. W. Dawes, 2004 Identification of a novel one-carbon metabolism regulon in *Saccharomyces cerevisiae*. *J. Biol. Chem.* 279: 7072–7081.
- Gerton, J. L., J. DeRisi, R. Shroff, M. Lichten, P. O. Brown *et al.*, 2000 Global mapping of meiotic recombination hotspots and coldspots in the yeast *Saccharomyces cerevisiae*. *Proc. Natl. Acad. Sci. USA* 97: 11383–11390.
- Goldfarb, T., and M. Lichten, 2010 Frequent and efficient use of the sister chromatid for DNA double-strand break repair during budding yeast meiosis. *PLoS Biol.* 8: e1000520.
- Grey, C., P. Barthes, G. Chauveau-Le Friec, F. Langa, F. Baudat *et al.*, 2011 Mouse PRDM9 DNA-binding specificity determines sites of histone H3 lysine 4 trimethylation for initiation of meiotic recombination. *PLoS Biol.* 9: e1001176.
- Hovring, I., A. Bostad, E. Ording, A. H. Myrset, and O. S. Gabrielsen, 1994 DNA-binding domain and recognition sequence of the yeast BAS1 protein, a divergent member of the Myb family of transcription factors. *J. Biol. Chem.* 269: 17663–17669.
- Hughes, T. R., and C. G. de Boer, 2013 Mapping yeast transcriptional networks. *Genetics* 195: 9–36.
- Jessop, L., T. Allers, and M. Lichten, 2005 Infrequent co-conversion of markers flanking a meiotic recombination initiation site in *Saccharomyces cerevisiae*. *Genetics* 169: 1353–1367.
- Kauppi, L., A. J. Jeffreys, and S. Keeney, 2004 Where the crossovers are: recombination distributions in mammals. *Nat. Rev. Genet.* 5: 413–424.
- Keeney, S., C. N. Giroux, and N. Kleckner, 1997 Meiosis-specific DNA double-strand breaks are catalyzed by Spo11, a member of a widely conserved protein family. *Cell* 88: 375–384.
- Keeney, S., and N. Kleckner, 1995 Covalent protein-DNA complexes at the 5' strand termini of meiosis-specific double-strand breaks in yeast. *Proc. Natl. Acad. Sci. USA* 92: 11274–11278.
- Keeney, S., and N. Kleckner, 1996 Communication between homologous chromosomes: genetic alterations at a nuclease-hypersensitive site can alter mitotic chromatin structure at that site both *in cis* and *in trans*. *Genes Cells* 1: 475–489.
- Kon, N., M. D. Krawchuk, B. G. Warren, G. R. Smith, and W. P. Wahls, 1997 Transcription factor Mts1/Mts2 (Atf1/Pcr1, Gad7/Pcr1) activates the *M26* meiotic recombination hotspot in *Schizosaccharomyces pombe*. *Proc. Natl. Acad. Sci. USA* 94: 13765–13770.
- Kugou, K., T. Fukuda, S. Yamada, M. Ito, H. Sasanuma *et al.*, 2009 Rec8 guides canonical Spo11 distribution along yeast meiotic chromosomes. *Mol. Biol. Cell* 20: 3064–3076.
- Kumar, R., H. M. Bourbon, and B. de Massy, 2010 Functional conservation of Mei4 for meiotic DNA double-strand break formation from yeasts to mice. *Genes Dev.* 24: 1266–1280.
- Lichten, M., 2008 Meiotic chromatin: The substrate for recombination initiation, pp. 165–193 in *Recombination and Meiosis*, edited by R. Egel and D. H. Lankenau. Springer-Verlag, Heidelberg, Germany.
- Lichten, M., and B. de Massy, 2011 The impressionistic landscape of meiotic recombination. *Cell* 147: 267–270.
- Lichten, M., and A. S. H. Goldman, 1995 Meiotic recombination hotspots. *Annu. Rev. Genet.* 29: 423–444.
- Liu, J., T. C. Wu, and M. Lichten, 1995 The location and structure of double-strand DNA breaks induced during yeast meiosis: evidence for a covalently linked DNA-protein intermediate. *EMBO J.* 14: 4599–4608.
- Machanick, P., and T. L. Bailey, 2011 MEME-ChIP: motif analysis of large DNA datasets. *Bioinformatics* 27: 1696–1697.
- MacIsaac, K. D., T. Wang, D. B. Gordon, D. K. Gifford, G. D. Stormo *et al.*, 2006 An improved map of conserved regulatory sites for *Saccharomyces cerevisiae*. *BMC Bioinformatics* 7: 113.
- MacQuarrie, K. L., A. P. Fong, R. H. Morse, and S. J. Tapscott, 2011 Genome-wide transcription factor binding: beyond direct target regulation. *Trends Genet.* 27: 141–148.
- Mancera, E., R. Bourgon, A. Brozzi, W. Huber, and L. M. Steinmetz, 2008 High-resolution mapping of meiotic crossovers and non-crossovers in yeast. *Nature* 454: 479–485.
- Mieczkowski, P. A., M. Dominska, M. J. Buck, J. L. Gerton, J. D. Lieb *et al.*, 2006 Global analysis of the relationship between the binding of the Bas1p transcription factor and meiosis-specific double-strand DNA breaks in *Saccharomyces cerevisiae*. *Mol. Cell. Biol.* 26: 1014–1027.
- Murakami, H., V. Borde, A. Nicolas, and S. Keeney, 2009 Gel electrophoresis assays for analyzing DNA double-strand breaks in *Saccharomyces cerevisiae* at various spatial resolutions. *Methods Mol. Biol.* 557: 117–142.
- Murakami, H., and S. Keeney, 2014 Temporospatial coordination of meiotic DNA replication and recombination via DDK recruitment to replisomes. *Cell* 158: 861–873.
- Myers, S., R. Bowden, A. Tumian, R. E. Bontrop, C. Freeman *et al.*, 2010 Drive against hotspot motifs in primates implicates the PRDM9 gene in meiotic recombination. *Science* 327: 876–879.
- Neale, M. J., J. Pan, and S. Keeney, 2005 Endonucleolytic processing of covalent protein-linked DNA double-strand breaks. *Nature* 436: 1053–1057.
- Ohta, K., T. Shibata, and A. Nicolas, 1994 Changes in chromatin structure at recombination initiation sites during yeast meiosis. *EMBO J.* 13: 5754–5763.
- Ohta, K., T. C. Wu, M. Lichten, and T. Shibata, 1999 Competitive inactivation of a double-strand DNA break site involves parallel suppression of meiosis-induced changes in chromatin configuration. *Nucleic Acids Res.* 27: 2175–2180.

- Padmore, R., L. Cao, and N. Kleckner, 1991 Temporal comparison of recombination and synaptonemal complex formation during meiosis in *S. cerevisiae*. Cell 66: 1239–1256.
- Pan, J., M. Sasaki, R. Kniewel, H. Murakami, H. G. Blitzblau *et al.*, 2011 A hierarchical combination of factors shapes the genome-wide topography of yeast meiotic recombination initiation. Cell 144: 719–731.
- Panizza, S., M. A. Mendoza, M. Berlinger, L. Huang, A. Nicolas *et al.*, 2011 Spo11-accessory proteins link double-strand break sites to the chromosome axis in early meiotic recombination. Cell 146: 372–383.
- Petes, T. D., 2001 Meiotic recombination hot spots and cold spots. Nat. Rev. Genet. 2: 360–369.
- Petronczki, M., M. F. Siomos, and K. Nasmyth, 2003 Un ménage à quatre: the molecular biology of chromosome segregation in meiosis. Cell 112: 423–440.
- Pokholok, D. K., C. T. Harbison, S. Levine, M. Cole, N. M. Hannett *et al.*, 2005 Genome-wide map of nucleosome acetylation and methylation in yeast. Cell 122: 517–527.
- Ponticelli, A. S., and G. R. Smith, 1992 Chromosomal context dependence of a eukaryotic recombinational hot spot. Proc. Natl. Acad. Sci. USA 89: 227–231.
- Ponticelli, A. S., E. P. Sena, and G. R. Smith, 1988 Genetic and physical analysis of the M26 recombination hotspot of *Schizosaccharomyces pombe*. Genetics 119: 491–497.
- Pratto, F., K. Brick, P. Khil, F. Smagulova, G. V. Petukhova *et al.*, 2014 DNA recombination. Recombination initiation maps of individual human genomes. Science 346: 1256442.
- Santiago, T. C., and C. B. Mamoun, 2003 Genome expression analysis in yeast reveals novel transcriptional regulation by inositol and choline and new regulatory functions for Opi1p, Ino2p, and Ino4p. J. Biol. Chem. 278: 38723–38730.
- Sasaki, M., S. E. Tischfield, M. van Overbeek, and S. Keeney, 2013 Meiotic recombination initiation in and around retrotransposable elements in *Saccharomyces cerevisiae*. PLoS Genet. 9: e1003732.
- Schuchert, P., M. Langsford, E. Kaslin, and J. Kohli, 1991 A specific DNA sequence is required for high frequency of recombination in the *ade6* gene of fission yeast. EMBO J. 10: 2157–2163.
- Schwacha, A., and N. Kleckner, 1994 Identification of joint molecules that form frequently between homologs but rarely between sister chromatids during yeast meiosis. Cell 76: 51–63.
- Schwank, S., R. Ebbert, K. Rautenstrauss, E. Schweizer, and H. J. Schuller, 1995 Yeast transcriptional activator INO2 interacts as an Ino2p/Ino4p basic helix-loop-helix heteromeric complex with the inositol/choline-responsive element necessary for expression of phospholipid biosynthetic genes in *Saccharomyces cerevisiae*. Nucleic Acids Res. 23: 230–237.
- Sommermeier, V., C. Beneut, E. Chaplais, M. E. Serrentino, and V. Borde, 2013 Spp1, a member of the Set1 Complex, promotes meiotic DSB formation in promoters by tethering histone H3K4 methylation sites to chromosome axes. Mol. Cell 49: 43–54.
- Stapleton, A., and T. D. Petes, 1991 The Tn3 beta-lactamase gene acts as a hotspot for meiotic recombination in yeast. Genetics 127: 39–51.
- Steiner, W. W., R. W. Schreckhise, and G. R. Smith, 2002 Meiotic DNA breaks at the *S. pombe* recombination hot spot M26. Mol. Cell 9: 847–855.
- Steiner, W. W., E. M. Steiner, A. R. Girvin, and L. E. Plewik, 2009 Novel nucleotide sequence motifs that produce hotspots of meiotic recombination in *Schizosaccharomyces pombe*. Genetics 182: 459–469.
- Sun, H., D. Treco, and J. W. Szostak, 1991 Extensive 3'-overhanging, single-stranded DNA associated with the meiosis-specific double-strand breaks at the *ARG4* recombination initiation site. Cell 64: 1155–1161.
- Thacker, D., N. Mohibullah, X. Zhu, and S. Keeney, 2014 Homologue engagement controls meiotic DNA break number and distribution. Nature 510: 241–246.
- Tischfield, S. E., and S. Keeney, 2012 Scale matters: the spatial correlation of yeast meiotic DNA breaks with histone H3 trimethylation is driven largely by independent colocalization at promoters. Cell Cycle 11: 1496–1503.
- Trapnell, C., B. A. Williams, G. Pertea, A. Mortazavi, G. Kwan *et al.*, 2010 Transcript assembly and quantification by RNA-Seq reveals unannotated transcripts and isoform switching during cell differentiation. Nat. Biotechnol. 28: 511–515.
- Wahls, W. P., and M. K. Davidson, 2010 Discrete DNA sites regulate global distribution of meiotic recombination. Trends Genet. 26: 202–208.
- White, M. A., M. Wierdl, P. Detloff, and T. D. Petes, 1991 DNA-binding protein RAP1 stimulates meiotic recombination at the *HIS4* locus in yeast. Proc. Natl. Acad. Sci. USA 88: 9755–9759.
- White, M. A., P. Detloff, M. Strand, and T. D. Petes, 1992 A promoter deletion reduces the rate of mitotic, but not meiotic, recombination at the *HIS4* locus in yeast. Curr. Genet. 21: 109–116.
- White, M. A., M. Dominska, and T. D. Petes, 1993 Transcription factors are required for the meiotic recombination hotspot at the *HIS4* locus in *Saccharomyces cerevisiae*. Proc. Natl. Acad. Sci. USA 90: 6621–6625.
- Wu, T.-C., and M. Lichten, 1994 Meiosis-induced double-strand break sites determined by yeast chromatin structure. Science 263: 515–518.
- Wu, T. C., and M. Lichten, 1995 Factors that affect the location and frequency of meiosis-induced double-strand breaks in *Saccharomyces cerevisiae*. Genetics 140: 55–66.
- Xu, L., and N. Kleckner, 1995 Sequence non-specific double-strand breaks and interhomolog interactions prior to double-strand break formation at a meiotic recombination hot spot in yeast. EMBO J. 14: 5115–5128.
- Zakharyevich, K., Y. Ma, S. Tang, P. Y.-H. Hwang, S. Boiteux *et al.*, 2010 Temporally and biochemically distinct activities of Exo1 during meiosis: double-strand break resection and resolution of double Holliday junctions. Mol. Cell 40: 1001–1015.
- Zhang, L., K. P. Kim, N. E. Kleckner, and A. Storlazzi, 2011a Meiotic double-strand breaks occur once per pair of (sister) chromatids and, via Mec1/ATR and Tel1/ATM, once per quartet of chromatids. Proc. Natl. Acad. Sci. USA 108: 20036–20041.
- Zhang, L., H. Ma, and B. F. Pugh, 2011b Stable and dynamic nucleosome states during a meiotic developmental process. Genome Res. 21: 875–884.
- Zhu, C., K. J. Byers, R. P. McCord, Z. Shi, M. F. Berger *et al.*, 2009 High-resolution DNA-binding specificity analysis of yeast transcription factors. Genome Res. 19: 556–566.

Communicating editor: N. Hunter

GENETICS

Supporting Information

www.genetics.org/lookup/suppl/doi:10.1534/genetics.115.178293/-/DC1

High-Resolution Global Analysis of the Influences of Bas1 and Ino4 Transcription Factors on Meiotic DNA Break Distributions in *Saccharomyces cerevisiae*

Xuan Zhu and Scott Keeney

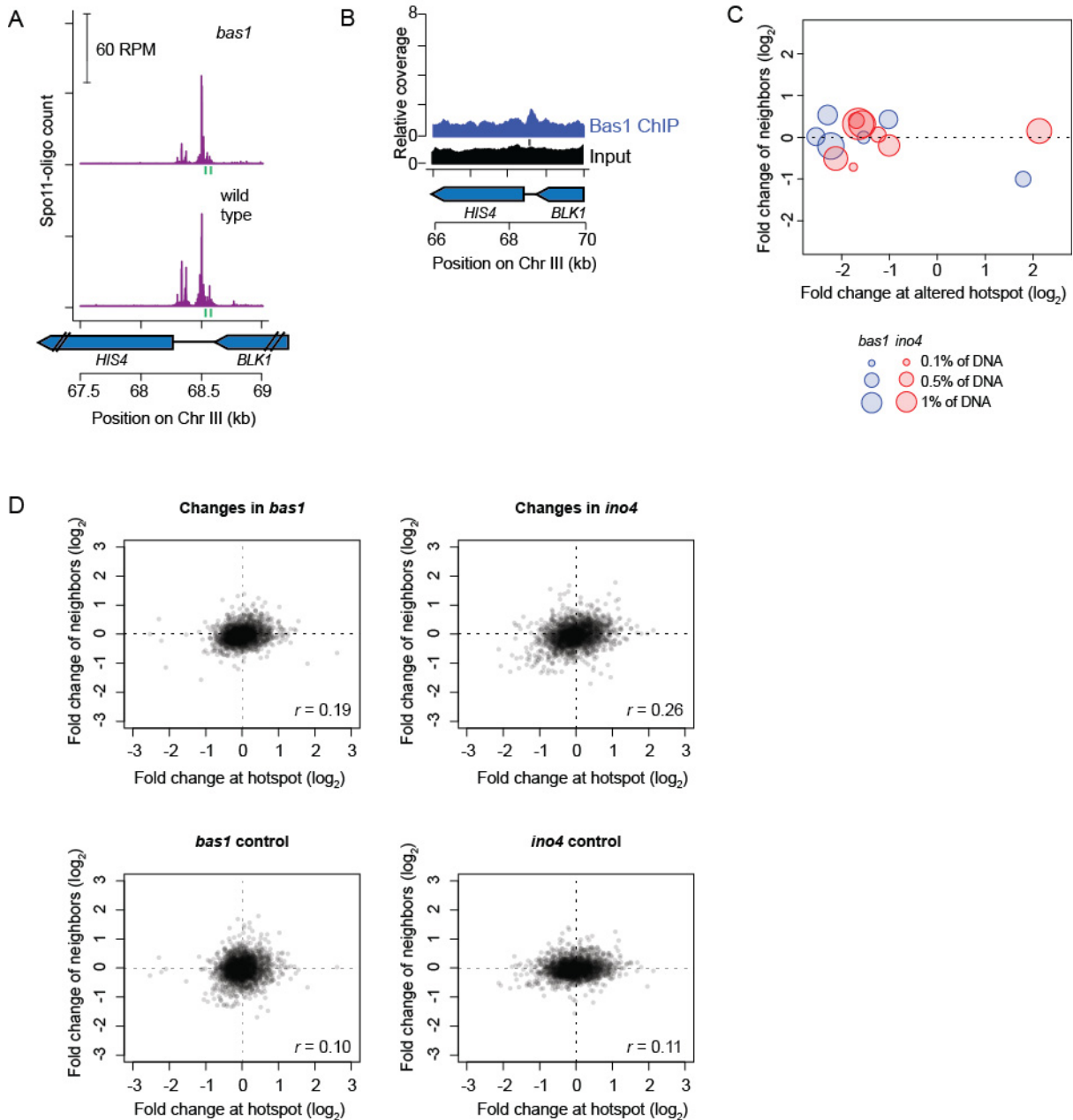


Figure S1 (A,B) Spo11 oligos (A) and Bas1 ChIP-seq signals (B) at the hotspot in the *HIS4* promoter. Green vertical ticks indicate matches to the Bas1 motif. *HIS4* is a modest hotspot in wild-type SK1 (870 RPM on average, equivalent to <2% of DNA broken; **Table S3**) and Spo11-oligo counts decrease to 64% of wild type in the *bas1* mutant (**Table S3**). A weak Bas1 ChIP-seq signal was discernible in the *HIS4* promoter, but was not sufficiently strong to pass our threshold for calling a Bas1 binding peak. (C,D) Hotspot competition is not a major contributor to altered DSB distributions in TF mutants. It is known that a very strong artificial hotspot can inhibit DSB formation at natural DSB hotspots nearby (see Main Text). Such behavior predicts that a hotspot whose intrinsic activity is altered by a TF mutation should show compensatory changes in the opposite direction for its neighbors: hotspots that decrease activity should show increased activity among the neighbors, and vice versa. The bubble plot in panel C compares the log fold change in Spo11-oligo counts at specific hotspots in *bas1* (blue) or *ino4* (red) mutants with the total log fold change of Spo11-oligo counts within the neighbors of those hotspots (within 5 kb on either side). Only hotspots that overlap ChIP-seq peaks of the respective TF, have ≥ 100 RPM average in at least one genotype, and show ≥ 2 -fold change of

Spo11-oligo count within the hotspot are shown. The area of each point is proportional to the Spo11-oligo count (i.e., DSB strength) in either wild type or the TF mutant, whichever was higher. There was no significant correlation between the change in these hotspots and the change in their neighbors ($p = 0.313$). Panel D is similar, but for all hotspots with ≥ 100 RPM average in at least one genotype. The top panels show fold changes in the *bas1* (left) or *ino4* (right) mutant. As controls for non-specific correlations, the bottom panels compare the fold change within each hotspot in one TF mutant with the fold change within the hotspot's neighbors in the other TF mutant. Only very weak positive correlations are seen, which is opposite the direction predicted for a hotspot competition effect. As discussed in the Main Text, it is likely that the lack of a signature of hotspot competition is because the hotspots whose activity changes have relatively low DSB frequencies, so their effects on their neighbors are too modest to be apparent when assayed in a cell population.

Table S1 Yeast strains

Strain number	Genotype
SKY3821	<i>MATa/MATα; ho::LYS2⁺; lys2⁻; ura3⁺; leu2⁻; arg4-Bgl^I; nuc1Δ::LEU2⁺; SPO11-His6-flag3-loxP-kanMX-loxP⁺</i>
SKY3860	<i>MATa/MATα; ho::LYS2⁺; lys2⁻; ura3⁺; leu2⁻; arg4-Bgl^I; nuc1Δ::LEU2⁺; SPO11-His6-flag3-loxP-kanMX-loxP⁺; bas1Δ::hphMX⁺; sae2Δ::NatMX⁺</i>
SKY3880	<i>MATa/MATα; ho::LYS2⁺; lys2⁻; ura3⁺; leu2⁻; arg4-Bgl^I; nuc1Δ::LEU2⁺; SPO11-His6-flag3-loxP-kanMX-loxP⁺; sae2Δ::NatMX⁺</i>
SKY4019	<i>MATa/MATα; ho::LYS2⁺; lys2⁻; ura3⁺; leu2⁻; arg4-Bgl^I; nuc1Δ::LEU2⁺; SPO11-His6-flag3-loxP-kanMX-loxP⁺; bas1Δ::hphMX⁺</i>
SKY4603	<i>MATa/MATα; ho::LYS2⁺; lys2⁻; ura3⁺; leu2⁻; arg4-Nspl^I; nuc1Δ::LEU2⁺; BAS1-myc13-KanMX⁺</i>
SKY4680	<i>MATa/MATα; ho::LYS2⁺; lys2⁻; ura3⁺; leu2⁻; arg4-Bgl^I; nuc1Δ::LEU2⁺; SPO11-His6-flag3-loxP-kanMX-loxP⁺; ino4Δ::hphMX⁺</i>
SKY4696	<i>MATa/MATα; ho::LYS2⁺; lys2⁻; ura3⁺; leu2⁻; arg4⁺; nuc1Δ::LEU2⁺; INO4-myc13-KanMX⁺</i>
SKY4846	<i>MATa/MATα; ho::LYS2⁺; lys2⁻; ura3⁺; leu2⁻; arg4⁺; nuc1Δ::LEU2⁺; SPO11-His6-flag3-loxP-kanMX-loxP⁺; ino4Δ::hphMX⁺; sae2Δ::NatMX⁺</i>

Table S2 Spo11-oligo sequencing statistics

Sample	Total sequenced	Total mapped^a	Total filtered^b	Uniquely mapped^c
wild type sample 1	4,361,438	4,302,910 (98.6%)	3,762,134 (86.2%)	3,633,091 (83.3%)
wild type sample 2	2,783,885	2,700,065 (97.0%)	2,360,467 (84.8%)	2,280,452 (81.9%)
<i>bas1</i> sample 1	5,615,623	5,545,624 (98.8%)	4,823,794 (85.9%)	4,665,416 (83.1%)
<i>bas1</i> sample 2	5,219,925	3,906,560 (74.8%)	3,212,796 (61.5%)	2,983,690 (57.2%)
<i>bas1</i> sample 3	5,410,693	5,349,120 (98.9%)	4,794,677 (88.6%)	4,542,315 (84.0%)
<i>bas1</i> sample 4	5,401,936	5,211,575 (96.5%)	4,540,169 (84.0%)	4,413,658 (81.7%)
<i>ino4</i> sample 1	3,241,998	3,203,647 (98.8%)	2,867,655 (88.4%)	2,664,527 (82.2%)
<i>ino4</i> sample 2	3,631,197	3,614,320 (99.5%)	3,188,652 (87.8%)	3,117,705 (85.9%)
<i>ino4</i> sample 3	4,160,807	4,127,194 (99.2%)	3,616,144 (86.9%)	3,480,102 (83.6%)

^a The fraction of sequences that could not be mapped likely reflect sequencing errors, adaptor dimers, PCR dimers and *bona fide* Spo11-oligos derived from genomic regions that are unique to SK1 (i.e., not found in the S288C reference strain).

^b Total number of reads that filtered to get rid of reads with poor alignment and/or adaptor clipping.

^c Total number of reads that mapped to only one position in the genome.

Tables S3-S7

Available for download as Excel files at www.genetics.org/lookup/suppl/doi:10.1534/genetics.115.178293/-/DC1

Table S3 Spo11-oligo hotspots called from a combined map merging the wild-type, *bas1* and *ino4* average maps

Table S4 Bas1 CHIP-seq peak positions and signals

Table S5 Ino4 CHIP-seq peak positions and signals

Table S6 RNA-seq differential gene expression in *bas1* mutants

Table S7 RNA-seq differential gene expression in *ino4* mutants